Ultrafast laser-induced control of magnetic anisotropy in nanostructures

© *A.M. Kalashnikova,*[1] *N.E. Khokhlov,*[1] *L.A. Shelukhin,*[1] *A.V. Scherbakov*[1,2]

[1] Ioffe Institute,
194021 St. Petersburg, Russia
[2] Experimental Physics II, Technical University Dortmund,
D-44227 Dortmund, Germany
e-mail: kalashnikova@mail.ioffe.ru

Employing short laser pulses with a duration below 100 fs for changing magnetic state of magnetically-ordered media has developed into a distinct branch of magnetism femtomagnetism which aims at controlling magnetization at ultimately short timescales. Among plethora of femtomagnetic phenomena, there is a class related to impact of femtosecond pulses on magnetic anisotropy of materials and nanostructures which defines orientation of magnetization, magnetic resonance frequencies and spin waves propagation. We present a review of main experimental results obtained in this field. We consider basic mechanisms responsible for a laser-induced change of various anisotropy types: magnetocrystalline, magnetoelastic, interfacial, shape anisotropy, and discuss specifics of these processes in magnetic metals and dielectrics. We consider several examples and describe features of magnetic anisotropy changes resulting from ultrafast laser-induced heating, impact of laser-induced dynamic and quasistatic strains and resonant excitation of electronic states. We also discuss perspectives of employing various mechanisms of laser-induced magnetic anisotropy change for enabling processes prospective for developing devices. We consider precessional magnetization switching for opto-magnetic information recording, generation of high-frequency strongly localized magnetic excitations and fields for magnetic nanotomography and hybrid magnonics, as well as controlling spin waves propagation for optically-reconfigurable magnonics. We further discuss opportunities which open up in studies of ultrafast magnetic anisotropy changes because of using short laser pulses in infrared and terahertz ranges.

Keywords: magnetic anisotropy, femtosecond laser pulses, femtomagnetism, picosecond acoustics, magnetization precession, spin waves, magnetization switching, magnon-phonon coupling.

Introduction

Magnetic anisotropy is the fundamental property of magnetically ordered materials, determining the technical aspect of the modern world. Due to the magnetic anisotropy, making the internal energy dependent on the magnetization direction, ferromagnets and ferrimagnets remain magnetized in zero external magnetic field. About 600 A.C. it led to the discovery magnetism as a phenomenon [1], and now it is a base for storing huge volumes of information on magnetic media without any energy costs. However, the data have to be recorded. In a modern informational world it must be done at the maximum possible speed and minimum energy costs. Implementation both these requirements is one of the principal fundamental and technical goals of the modern magnetism science.

One of the ways for magnetization control is to manage magnetic anisotropy. Apparently, it is the oldest and continuously developing method applied by humanity for controlling the magnetic order. As far back as the 18th century, the shape anisotropy was a key technical factor in the manufacture of steel magnets. Their shape determined durability and permanence of magnetic prop-

erties [2]. Experiments performed in the second half of the 19th century by James Joule [2] and Emilio Villari [3] discovered a relation between the magnetization direction and symmetry of the crystal lattice, determined by the magnetocrystalline anisotropy. Control of its parameters through the selection of the magnetic material composition is the main method to make the required properties of a magnetic alloy, and sensibility to deformation is the technical basis for magnetomechanical and thermomagnetic devices [4]. The possibility of layer-by-layer growth of thin magnetic layers came with the development of epitaxial technologies, enabled using anisotropy of interfaces in magnetic microstructures [5]. Finally, modern technologies of molecular growth and nanolithography with the sub-nanometer accuracy, allow us to tune parameters of magnetic anisotropy of nanostructures at the atomic level, by combining all the above mentioned approaches.

Ultrafast tools are required for the subpicosecond magnetization management. Such a tool, available to researches and engineers for the recent 20 years is femtosecond lasers. The first successful experiment with the laser pulse shorter than 1 ps affecting a ferromagnet was performed in 1996 [6]. It showed the possibility to modify the magnetization of a ferromagnet at the

rate, earlier believed as totally unreal. That experiment significantly expanded the concepts of the magnetic order control and discovered the universe of ultrafast magnetic phenomena. Now the impact of laser pulses on magnetically ordered materials is the subject of an individual discipline — femtomagnetism. Its general progress is given in a series of review papers [7–9]. Optically induced change of magnetic anisotropy is one of the subjects of active studies within the framework of this discipline.

A diversity of the types of magnetic anisotropy is a result of the variety of interactions determining it, such as dipole-dipole, spin-orbit, and exchange. Absorption of the ultrashort optical pulse by a material affects all its subsystems, such as charge carriers, phonons, spin system. A portion of the optical pulse energy will be transmitted to each of these subsystems at some rate and efficiency. Consequently, laser pulse is able to affect all types of interactions and engage all the known mechanisms for magnetic anisotropy control. Moreover, a technological capability to tune the composition, shape, and morphology of a complex magnetic structure allows providing the targeted and controllable effect of laser pulses on magnetic anisotropy. Importantly, it happens at timescale inaccessible by any other alternative method. The goal of this review is to present a full diversity of experimental effects related to the impact of laser pulses of optical and near infrared ranges on the magnetic anisotropy of magnetically ordered materials. In this review, we limit our consideration by ferromagnetic and ferrimagnetic, as well as weak ferromagnetic materials, i.e. with a macroscopic magnetization in zero external magnetic field. However, in the general case, such effects can also be realized in materials without macroscopic magnetization. We will consider the main results of fundamental research and try to highlight promising approaches from the point of view of solving of specific applied problems of the ultrafast magnetism. In addition, we will discuss the emergence of a new direction in the research of ultrafast changes in magnetic anisotropy, using pulses of the mid-infrared and terahertz ranges.

The review is structured as follows. Sect. 1 presents a theoretical base, used for description of the results of ultrafast experiments. In Sect. 2 we discuss the fundamentals of the experimental study of the effects of laser pulses on magnetic anisotropy. Sect. 3 is devoted to the main experimental manifestations corresponding to various mechanisms of such effect. Sect. 4 represents the most interesting experiments in terms of applications and perspectives of the further development of that field of femtomagnetism are discussed. In the Conclusion we also consider what prospects in the field of research of ultrafast magnetic anisotropy changes are opened by the use of short pulses of the infrared and terahertz ranges.

1. Magnetic anisotropy of bulk materials and nanostructures

1.1. Phenomenological description of magnetic anisotropy

From the phenomenological point of view, availability of magnetic anisotropy in a ferromagnet is described by the introduction of additional even-order magnetization elements **M**:

$$W_A = \begin{cases} K_u m_z^2 + \dots \\ K_1(m_x^2 m_y^2 + m_x^2 m_z^2 + m_y^2 m_z^2) + \dots \end{cases}, \quad (1)$$

where $\mathbf{m} = \mathbf{M} M_S^{-1}$ is the unit vector co-directional to the magnetization, M_S is the saturation magnetization. The coefficients in the expansion K have a physical dimension of the energy density and are called magnetic anisotropy parameters. The difference from zero of one or another K parameter in the expression for the anisotropy energy (1) is determined both by the crystal symmetry of the material and its shape.

An uniaxial magnetic anisotropy described by the second-order magnetization invariant in (1) is inherent for bulk ferromagnets with crystal structure featured by the preferred z axis of symmetry, as well as for magnetic micro- and nanoobjects, whose shape has such axis. Uniaxial anisotropy is characterized by the presence of easy (at $K_u < 0$) or the hard (at $K_u > 0$) magnetization axis, aligned with the z-axis. In this case, in the plane perpendicular to the easy (hard) z axis, materials also could have additional anisotropy described by the elements of higher m_i orders. The specific form of the additional terms is determined by the symmetry of the crystal. Without discussing in detail herein the anisotropy features of crystals with anisotropy of crystals with various symmetries, we refer the reader to the classical books [10,11].

Materials with cubic crystal lattice demonstrate the cubical magnetic anisotropy described by the fourth-order invariant in the (1). Axes of easy magnetization in materials with cubical anisotropy can be either spatial diagonals (at $K_1 < 0$), or cube edges (at $K_1 > 0$). The next element in the expansion (1) for such materials is the 6th order magnetization element. Note that the description of magnetic anisotropy given above is also applicable to ferrimagnets, antiferromagnets, and weak ferromagnets, etc. In the case of antiferromagnet and weak ferromagnet, one can write invariants similar to (1), containing expansion by even degrees of the antiferromagnetic unit vector.

Equilibrium orientation of magnetization in a ferromagnet placed into the external magnetic field $\mathbf{H}_{\text{ext}}$ is determined by the balance between the magnetic anisotropy energy W_A and the Zeemann energy $W_H = -\mathbf{M}\mathbf{H}_{\text{ext}}$. In the general case, the efficient field is introduced for the description of the equilibrium orientation of magnetization

$$\mathbf{H}_{\text{eff}} = -\frac{\partial W}{\partial \mathbf{M}}, \quad (2)$$

where $W = W_A + W_H$ is the full magnetic energy. If only the energy of magnetic anisotropy $W = W_A$ is considered, i.e. without the external magnetic field, then the expression (2) allows to obtain the efficient field of magnetic anisotropy $\mathbf{H}_A$ co-directional with the easy magnetization axis. Its value is determined as $H_A \sim -nKM_S^{-1}$ with the accuracy up to the n multiplier determined by the invariant degree in the expansion (1); $n = 2, 4$ for uniaxial and cubic anisotropy, respectively. Full efficient field is the vector sum of the efficient field of anisotropy $\mathbf{H}_A$ and external magnetic field $\mathbf{H}_{ext}$.

In case of more complex media with two and more magnetic sublattices there are additional contributions related to the exchange interaction between sublattices. In this case orientation of magnetizations of sublattices depends on the balance between the exchange energy, anisotropy energy and the Zeemann energy manifested, in particular, as the spin-flop effects in ferri- and antiferromagnets, and spin flips in antiferromagnets in the external magnetic field. When describing such materials, one may introduce efficient fields of exchange and anisotropy acting on each sublattice, or use the term of staggered field on the magnetic cell scale affecting the antiferromagnetic vector.

1.2. Mechanisms of magnetic anisotropy emergence

The above mentioned phenomenological discussion associates magnetic anisotropy exclusively with the crystal symmetry or shape of the magnetic material and is applicable to the description of anisotropy occurring as a result of various microscopic interactions. It is convenient to divide the microscopic mechanisms of the magnetic anisotropy emergence in two types: single- and two ion ones. According to the names, in the first case, the interactions determining anisotropy of magnetic properties of material are determined by the energy of a single magnetic ion in certain crystal surrounding. In the second case, anisotropy is a result of magnetic ion interaction with other magnetic ions. We shortly describe the main microscopic mechanisms of magnetic anisotropy and susceptibility of anisotropy types to main external impacts — temperature, mechanical strains, and electrical fields.

In the majority of magnetic crystals, the dominating interaction, which determines the magnetic anisotropy, is spin-orbit interaction $W_{S-O} = -\lambda_{S-O}\mathbf{S} \cdot \mathbf{L}$, by which the ion spin moment $\mathbf{S}$ appears to be sensitive to its crystal surrounding that defines orientation of the orbit moment $\mathbf{L}$. Such interaction between the spin and orbit moments of one ion determines single-ion magnetocrystalline anisotropy. An absolute value of the parameter of single-ion magnetic crystal anisotropy K depends also on the parameter of spin-orbit coupling λ_{S-O}, and on the value of orbit moment of the ion $\mathbf{L}$ [12,13]. Relation of K with the value of orbit moment $\mathbf{L}$ is clearly

demonstrated by the case of rare earth metals and compounds based on them featuring high magnetocrystalline anisotropy [11].

It is important to note that for magnetocrystalline anisotropy the angular moment „freezing" plays a key role. For example, ground state of the Fe^{3+} ion in octahedral surrounding is the s-state with frozen, i.e. null angular moment $\mathbf{L} = 0$. This phenomenon determines a relatively low magnetocrystalline anisotropy of the Fe^{3+} iron ions compounds, including many of oxides. A considerably higher value K is an indicative for the Co^{2+} compounds with $L \neq 0$ in comparison with Fe^{3+}-based materials, which is analyzed in detail, for example, for cobalt ferrite spinels [15].

In addition to magnetocrystalline anisotropy spin-orbit interaction determines such types of anisotropy as magnetoelastic, growth-induced and surface anisotropy playing a key, and often determinant role in the magnetic properties of thin and ultrathin films, hetero- and nanostructures. Magnetoelastic contribution to anisotropy is manifested when deformations emerge in the material, caused by the application of external forces or associated with the magnetic sample growth. This effect is known as inverse magnetostriction. For a cubic ferromagnet, the change of magnetic energy in the presence of tensile/compression deformations ϵ_{ii} and shear deformations ϵ_{ij} is described as

$$W_{M-E} = B_1(\epsilon_{xx}m_x^2 + \epsilon_{yy}m_y^2 + \epsilon_{zz}m_z^2)$$
$$+ 2B_2(\epsilon_{xy}m_xm_y + \epsilon_{xz}m_xm_z + \epsilon_{yz}m_ym_z + \ldots), \quad (3)$$

where B_1, B_2 are magnetoelastic parameters. Magnetoelastic parameters B are connected with the magnetostriction coefficients $\lambda_{100}, \lambda_{111}$ measured in experiments through the expressions $\lambda_{100} = 2/3B_1(c_{12} - c_{11})^{-1}$ and $\lambda_{111} = -1/3B_2c_{44}^{-1}$, where c_{11}, c_{12}, c_{44} are elastic stiffness coefficients. Indices of the coefficients λ indicate crystallographic direction the sample was magnetized during the measurement of the magnetostriction effect. The same as the parameters of magnetocrystalline anisotropy K, magnetoelastic parameters B can also have different signs depending on the material.

With the development of thin film and nanostructure technologies, the study of deformations effect on the magnetic properties of such structures entered on a new stage. On the one hand, deformations occurring, for example, due to the mismatch of lattice constants of different components of epitaxial heterostructures or due to different thermal expansion coefficients of the components, may result in modifications of magnetic properties by compensating or supplementing other contributions into magnetic anisotropy. On the other hand, deformations can be created intentionally and controllable at the stages of growth or post-growth processing of hetero- and nanostructures, in order to manage their magnetic properties. It is the subject of studies in the field of straintronics and deformations engineering [14]. For example, deformations in heterostructures can be used for

the creation of indirect coupling between magnetization of one of the heterostructure layers with any of the parameters of another layer. A good example of such deformations engineering is implementation of indirect magnetoelectric relation in synthetic multiferroics — heterostructures consisting of layers of magnetic and ferroelectric materials [14,15]. Deformations in such structures associated with the value and direction of spontaneous polarization **P** of ferroelectric layers are transmitted through the interface into a magnetic layer, modifying its anisotropy [16] and result in switching of magnetization **M** when **P** changes direction [17].

In addition to single-ion contribution associated with spin-orbit coupling, the magnetic dipole-dipole interaction can also contribute to magnetocrystalline and magnetoelastic anisotropy. It determines the dependence of the magnetic moments system energy on their orientation relative to the radius-vector between them. Such a contribution, apparently, is an example of the two-ion anisotropy term. However, in the majority of solid materials it appears to be considerably lower than the spin-orbit interaction. In case of magnetic anisotropy of thin films, micro- and nanostructures, the role of magnetic dipole-dipole interaction grows. In these structures the most important contribution to anisotropy is made by so called shape anisotropy, emerging as a result of minimization of scattered magnetic fields created by the magnetized material. Thus, for a thin laterally extended film, the energy of shape anisotropy is determined as

$$W_S = 0.5\mu_0 M_S^2 m_z^2, \qquad (4)$$

where the axis z matches the surface normal, μ_0 is the magnetic permittivity of vacuum. According to expression (4), shape anisotropy for thin film is the „hard axis" type with efficient parameter $K_u = 0.5\mu_0 M_S^2 > 0$. Since K_u in this case depends on saturation magnetization, the shape anisotropy often dominates in thin films of ferromagnetic metals with high M_S. For laterally limited thin film structures the minimization of scattered fields could result in the formation of spatially heterogeneous distributions of magnetization, for example, magnetic vortices in micron magnetic discs [18].

One more significant factor affecting magnetic anisotropy of thin films, hetero- and nanostructures is the presence of interfaces between magnetic material and air or other material, both magnetic, and non-magnetic. Magnetic ion at epitaxial interface is affected by modified crystal field, as a rule, with low symmetry. Based on the phenomenological consideration, this may result in local modification of the magnetic anisotropy type. As a result of change of symmetry and the value of crystal field, the energy of spin-orbit interaction is changed for magnetic ions at the interface, their orbit moment becomes „defrosted" monocrystalline anisotropy is locally modified, accordingly, and so called interface anisotropy appears, which can considerably differ from bulk [5]. Because of symmetry, the interface anisotropy

is uniaxial, even if the material has, for example, cubic anisotropy in the bulk. In ultrathin films of ferromagnetic metals with the thickness d, neighboring to oxides, the „easy axis" type of the interface anisotropy energy

$$W_I = \frac{K_I}{d} m_z^2 \qquad (5)$$

competes with the shape anisotropy energy W_S (4). Here $K_I < 0$ is the interface anisotropy parameter having the dimension of the surface energy density. If $|K_I|d^{-1} > 0.5\mu_0 M_S^2$, then the condition of perpendicular magnetic anisotropy (PMA) stabilization is met, and easy magnetization direction is normal to the film surface. The PMA stabilization considerably affected by crystal structure of the neighboring layer and how it is termed indicate a key role of the magnetic ion surrounding at the interface for the interface anisotropy emergence. Note that the last studies show that the contribution to interface anisotropy appears to be not exclusively single-ion. Two-ion contributions emerging as a result of modified exchange and dipole-dipole interaction between interface magnetic ions also affect the resulting magnetic anisotropy [19].

A special case refers to structures with the interface between the magnetic and nonmagnetic layer with a strong spin-orbit coupling, for example, platinum (Pt). In this case, in addition to modification of the strength and type of magnetic anisotropy, and, for example, PMA stabilization, the Dzyaloshinskii-Moriya interaction begins playing a great role in the near-to-interface layer, and noncollinear magnetic structures, including skyrmions, can appear [20]. Regarding the boundary between two magnetically ordered materials, the exchange interaction between interface ions from different layers also contributes to the formation of magnetic state resulting in such phenomena as exchange bias at the ferromagnet/antiferromagnet boundary [21].

1.3. Changes of magnetic anisotropy under effect of external factors

Such external factors as the temperature, pressure and deformation, electrical field result in changes of magnetic anisotropy. Thus, in case of a simple ferromagnet, the temperature increase results in the decrease of magnetization, as well as in reduction of the magnetic anisotropy parameters K. And the change of K with the temperature increase is faster than the saturation magnetization M_S change at the temperatures far from the Curie temperature T_C. Theoretical description of temperature changes of the single-ion magnetocrystalline anisotropy parameter was obtained in [22]. Similar approach was also applied to magnetoelastic anisotropy [23,24]. Theoretical description was obtained in the model, when the energy required for reorientation of magnetic moment of one ion from the easy to hard axis, does not depend on the temperature. And the range of angles characterizing

directions of magnetic momenta of different ions rises with an increase of the temperature. This results, in turn, in an increase of the magnetic energy in the situation when the average magnetic moment of magnetic ions, i.e. magnetization, is oriented along the easy axis, and in reduction of that energy, when magnetization is oriented along the hard direction. The research [22] and further works showed that the nature of temperature dependence $K(T)$ is determined by type of magnetocrystalline anisotropy the material, and the following expression was derived

$$\frac{K(T)}{K(0)} = \left[\frac{M_S(T)}{M_S(0)}\right]^{\frac{n(n+1)}{2}}, \qquad (6)$$

where $K(0)$ and $M_S(0)$ is the parameter of magnetocrystalline anisotropy and the saturation magnetization at $T = 0\,\mathrm{K}$, n is the expansion order in the expression for the magnetic anisotropy energy (1). Therefore, the parameter of uniaxial anisotropy K_u varies with the temperature as M_S^3, and cubic anisotropy K_1 — as M_S^{10}.

Changes of the nonsingle-ion magnetic anisotropy parameter with temperature, in general case, also obeys the power law, however, with other values of the degree. Thus, for two-ion uniaxial magnetic anisotropy, the degree is close to 2. An obvious example is the shape anisotropy (4) with efficient parameter K_u proportional M_S^2. Note that the study of temperature dependences of the magnetic anisotropy parameter is also used for the determination of dominating contributions to anisotropy [19].

Because of the inverse magnetostriction described in sect. 1.2, one more external factor influencing the magnetic anisotropy of materials is the pressure and creation of tensile/compression or shear strain. Moreover, since the source of magnetocrystalline anisotropy is the effect of crystal fields on the orbit moment, and, through the spin-orbit interaction, on spin moments, application of external electrical field is one more efficient approach to the change of magnetic anisotropy of materials.

Co-existence of two and more sources of magnetic anisotropy can result in a non-trivial response of magnetic material to external effects. A good demonstration of such response is spin-reorientation (SR) phase transitions in bulk materials, for example, rare earth orthoferrites $REFeO_3$, where RE is the rare-earth ion. In $REFeO_3$, there is a competition between single-ion contribution to anisotropy of the Fe^{3+} ion and two-ion, occurring due to exchange interaction between Fe^{3+} and RE^{3+} ion, demonstrating a strong dependence of the magnetic moment on the temperature [25,26]. As a result, at certain temperatures depending on the RE^{3+} ion type, the anisotropy axis reorients to $90°$ from the direction at low temperatures defined by the Re^{3+} to the Fe^{3+} determined axis. The SR-transition is also implemented in ultrathin ferromagnetic films due to the change of balance between the shape anisotropy and the interface anisotropy [27–29].

Optical radiation is also an external effect, which allows to modify the magnetic anisotropy. The latter can be based both on such optical excitation non-specific mechanisms as heating or deformation, and on the optical-specific mechanisms, for example, resonant excitation of ions responsible for magnetic anisotropy [30]. Using of short, pico- and subpicosecond laser pulses brought the study of optically induced modifications of magnetic anisotropy to a further stage.

2. Experimental study of laser induced modifications of magnetic anisotropy

There are a lot experimental methods for measurement of the parameters of magnetic anisotropy parameters in equilibrium state. Among them the ferromagnetic resonance [31] is one of the most common, where the anisotropy field is estimated based on the ferromagnetic resonance frequency measured in the experiment [10]. The Mandelstam-Brillouin light scattering (BLS) method allows to measure magnetic anisotropy locally from the spectrum of spin waves [32]. Moreover, the type and parameters of anisotropy can be obtained by measuring field dependences of magnetization along hard axis, and determining saturation fields proportional to KM_S^{-1} using the vibration [33], and the SQUID-magnetometry [34], as well as the magnetooptical (MO) magnetometry [35].

For the study of magnetic anisotropy change with femtosecond laser pulses it is necessary to measure its evolution at a few picosecond timescale and less. The methods mentioned above do not enable measurements with such a time resolution. The most universal method for study ultrafast laser-induced change of the magnetic state of various materials and structures is femtosecond MO pump-probe. It is the measurement with a high temporal resolution of the MO response to femtosecond laser excitation. However, the MO effects are not directly connected with the parameters of magnetic anisotropy of a material, and proportional to certain magnetization projections [35]. Therefore, information on the laser-induced change of magnetic anisotropy in MO pump-probe experiments one can get using approach considered in many works as the time-resolved ferromagnetic resonance measurement.

The main principle of such measurements is shown in Fig. 1, a. In a non-excited medium the magnetization is oriented along the effective field $\mathbf{H}_{\mathrm{eff}}$ (2). If magnetic anisotropy modification occurs as a result of the effect of laser pulse, then, in the general case, orientation and value $\mathbf{H}_{\mathrm{eff}}$ do not persist. If the change of orientation $\mathbf{H}_{\mathrm{eff}} \to \mathbf{H}'_{\mathrm{eff}}$ occurs fast enough, then magnetization does not follow effective field direction. Therefore, as a result of the laser pulse action, the state of the material is characterized by the noncollinearity magnetization and modified $\mathbf{H}'_{\mathrm{eff}}$. Evolution
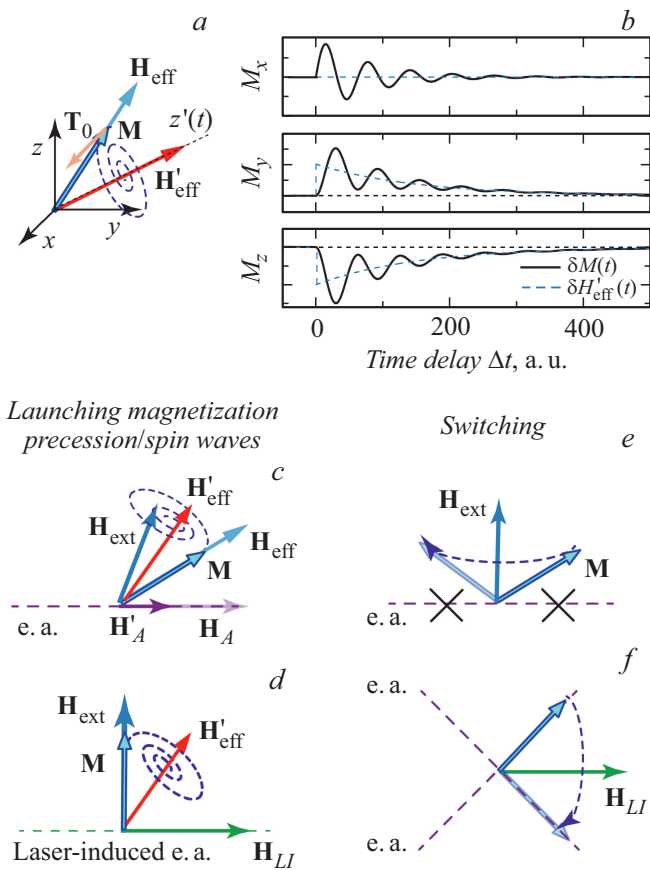
Figure 1. a — magnetization precession excitation as a result of laser-induced modification of total effective field $\mathbf{H}_{\mathrm{eff}} \to \mathbf{H}'_{\mathrm{eff}}$; b — corresponding evolution of magnetization projections $\{M_x, M_y, M_z\}$. Schematic diagram of the magnetization trajectory (c, d) due to the excitation of magnetic precession and (e, f) in case of magnetization switching as a result of reduction of the magnetic anisotropy parameter K (c, e) or emergence of the efficient field of laser-induced anisotropy $\mathbf{H}_{LI}$; e.a. — easy magnetization axis.

of magnetization orientation in this case is described by the Landau-Lifshitz (LL) equation [36]:

$$\frac{d\mathbf{M}}{dt} = -\gamma \mathbf{M} \times \mathbf{H}'_{\mathrm{eff}} - \gamma \frac{\alpha}{M}\mathbf{M} \times (\mathbf{M} \times \mathbf{H}'_{\mathrm{eff}}), \qquad (7)$$

where γ is the gyromagnetic ratio for electrons in magnetic ion. The first term in the right part of the equation describes precession motion of magnetization with the frequency $f = \gamma H'_{\mathrm{eff}}$. The second element describing the precession damping is given in the Hilbertian form with parameter α [37].

Therefore, as a result of change of direction $\mathbf{H}'_{\mathrm{eff}}$, according to (7), magnetization is affected by the torque $\mathbf{T} = d\mathbf{M}dt^{-1}$, leading to the magnetization precessing around $\mathbf{H}'_{\mathrm{eff}}$. In Fig. 1, a it is clearly seen that the direction of $\mathbf{T}$ is determined by new direction of effective field. Using the information about $\mathbf{T}$, we can reconstruct the behavior of $\mathbf{H}_{\mathrm{eff}}$, including the change of $\mathbf{H}_A$ immediately after the

laser excitation. Moreover, magnetization precesses around $\mathbf{H}'_{\mathrm{eff}}$ being a function of time due to the material relaxation from excited state to equilibrium. By tracking the precession frequency and trajectory, we get information about these processes.

Note that modification of $\mathbf{H}_{\mathrm{eff}}$ under the laser excitation may occur both as a result of changes of the anisotropy parameters K, and emergence of new axes of anisotropy with corresponding effective field $\mathbf{H}_{LI}$ (see Fig. 1, c, d). Distinguishing of such processes in experiments is an important task, since fundamentally different microscopic mechanisms determine them, as shown in the next section.

Therefore, the detection of ultrafast change of magnetic anisotropy assumes experimental measurement of the laser-induced magnetization trajectory. In practice, the detection of precession is implemented in the MO pump-probe method [7], when the magnetization dynamics in the medium is excited by a powerful femtosecond laser pulse, and then the change of diffenent magnetization projections in the pumped area are probed by the measurement of the MO effects for weak linearly polarized probe pulse delayed relative to the pump for the time Δt. Various MO effects manifested as the rotation of the polarization plane, emergence of ellipticity or change of the probe pulse intensity [35] are proportional to different magnetization projections. Therefore, in general case, one can get comprehensive information about the magnetization orientation at the moment of the probe pulse interaction with the sample [38]. By changing the delay time Δt between the pump and probe pulses, one may track the dynamics of one or several magnetization projections. Thus, the time resolution is determined by the duration of the probe pulse. However, from the point of view of the anisotropy change, efficient time resolution of such experiment is limited by the precession frequency. For example, if the time of laser-induced magnetic anisotropy change, is considerably lower than the precession period, then the information about this cannot be obtained from the experiment, and phenomenologically anisotropy change is described by the Heaviside function.

Fig. 2 shows an example of a two-color ultrafast MO pump-probe setup, where the MO Kerr effect is measured as the function of delay time Δt between the pump and probe pulses. Note that in the majority of experiments the information about laser-induced magnetization precession trajectory is successfully restored using data on time evolution only of one of the magnetization components and modeling based on the LL equation (7) or linearized LL equation [39,40] in case of low precession amplitudes. In a typical experiment, averaging is performed by a high number of pump-probe events for each delay time. Therefore, it is important that after the each event the system is relaxed to the same initial condition between the probe and next pump pulse. This is why the measurements are performed in the external magnetic field determining the initial magnetization orientation, and the pulse repetition period should be longer than the relaxation time.
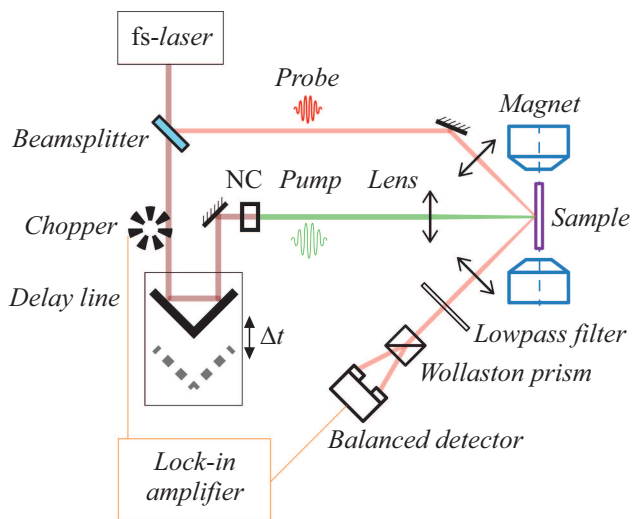
Figure 2. Example of a block diagram of a femtosecond MO pump-probe setup. The pump and probe pulses are focused on the sample surface placed in the external magnetic field, by lens or a microobjective. In the presented configuration, the Kerr MO rotation of the probe pulse polarization is measured as the function of delay time Δt between the pump and probe pulses. The measurement of the polarization plane rotation is performed by polarimetric scheme consisting of the Wollaston prism and balance photodetector. Variable time delay Δt between the pump and probe pulses is provided by the change of the optical path length of the pump pulse with mechanical delay line with a retroreflector installed on it. In the general case, the probe pulse photon energy may differ from the pump, for example, due to doubling energy with non-linear optical crystal NC. Herein a part of the pump pulses is blocked by chopper with the frequency used as a reference in a lock-in amplifier demodulating the signal received from the photodetector.

An exclusion is the experiments,where high repetition rate are selected intentionally so, for example, that each next pump pulse amplified the effect from the previous. A special approach is also applied for the study of laser-induced switching of magnetization, where a single-pulse pump-probe method is implemented, enabling separate detection of the effect of each pump pulse.

3. Main mechanisms and demonstration of ultrafast anisotropy changes

3.1. Laser-induced heating

An obvious mechanism of the laser-induced change of the magnetic anisotropy is laser-induced heating, since the magnetic anisotropy parameters demonstrate the temperature dependence (see sect. 1.3). However, the specific scenario of the magnetic anisotropy modification resulting from laser-induced heating depends on the electron structure of a magnetic material and what subsystems are involved to the femtosecond laser pulse energy absorption.

The most fundamental difference refers to ultrafast laser-induced heating in magnetic metals and dielectrics. The process of femtosecond laser pulse energy absorption in a metal can successfully be described by so called two-temperature model, suggesting that the laser pulse excitation results in a fast and significant increase of the efficient temperature of conductivity electrons (Fig. 3, c). Further, time of the electron system temperature rise does not exceed 100 fs, and the achieved temperatures are $\sim 500-1000$ K because of a low heat capacity of the electron gas. Thermalization of electron and phonon subsystems occur at a timescale about several picoseconds and more. Due to a high heat capacity of the phonon subsystem, the lattice heating is much lower than for electrons, being ~ 100 K.

In a magnetic metal, ultrafast heating of electron and phonon subsystems results in the emergence of the ultrafast demagnetization [6]. Specific times of that process make ~ 100 fs for $3d$-metals, because the $3d$ shell electrons, hybridized with the conductivity $4sp$-electrons, determine the magnetic order. On the contrary, in $4f$-metals, ultrafast demagnetization is much lower, because magnetism is determined by electrons of the $4f$-shell, not hybridized with $5d6sp$-electrons absorbing the laser pulse energy. As a result, demagnetization in such materials features longer times ~ 100 ps and is associated with the lattice heating. The details of ultrafast demagnetization in metals and the current state of the theory of this process are discussed in the works [41–43].

Energy absorption in magnetic dielectrics in visible and near infrared ranges is mainly occurs due to the excitation
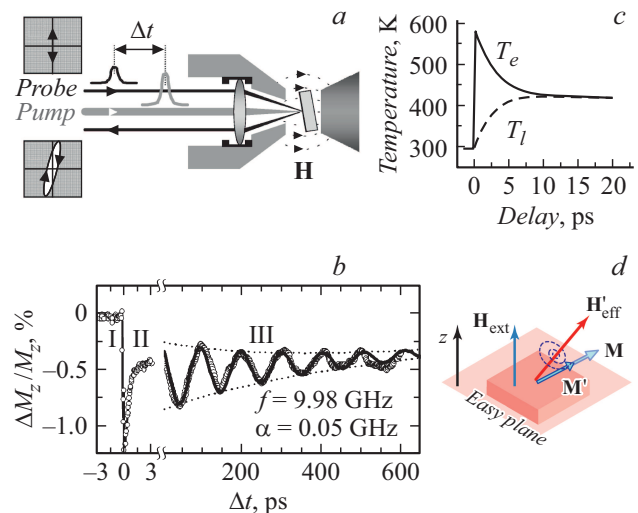

Figure 3. a — magnetic optical pump-probe setup for monitoring of the laser-induced magnetization precession in a thin film of Ni; b — signal showing modifications of the magnetization component out of plane M_z as a function of the delay time Δt between pump and probe pulses [45]; c — example of the temperature dependence of the T_e electron subsystem and the T_l lattice on the delay time between pump and probe pulses calculated for Co [46]; d — scheme of the magnetic precession excitation process as a result of laser-induced modification of the shape anisotropy. (Figures are reproduced from [45] (a, b) and [46] (c).)

of localized transitions with further emissionless relaxation accompanied by the energy transfer to the lattice at the times below picosecond. Laser-induced demagnetization has characteristic times ~ 100 ps [44].

3.1.1. Laser-induced heating in metals

According to discussions in sect. 1.3, the shape anisotropy (4) and corresponding effective field $\mathbf{H}_S = -\mu_0 M_S \mathbf{m}_z$ depend on saturation magnetization M_S. Ultrafast demagnetization results in the change of magnetic anisotropy of thin films of ferromagnetic and ferrimagnetic metals just by the modification of the shape anisotropy. For observation of this effect experimental geometry is required when equilibrium magnetization, i.e. before the femtosecond laser pulse excitation, has a non-zero projection on the film surface normal, for example, when the external magnetic field is applied along the normal. In this case, laser-induced reduction of saturation magnetization $\Delta M_S(t)$ results in a change of the direction of the total effective field $\mathbf{H}_{eff}$, namely, to an increase of its projection on the normal with the value proportional to $\Delta M_S(t)$, and to the excitation of precession according to the scheme given in Fig. 3, d.

This approach was applied in the work [45], where the experimental observation of laser-induced precession of magnetization was achieved for the first time. In this work laser-induced dynamics of the magnetization M_z projection to the normal of Ni film with the thickness of 7 nm (Fig. 3, a) was measured. Three time ranges were distinguished in the dynamics of the magnetization measured in the experiment (Fig. 3, b). Fast reduction of M_z is observed within the range of I $(0-1$ ps$)$ due to ultrafast demagnetization. There is partial magnetization restoration in range II, and in range III — magnetization precession. Importantly, in the transient region between ranges II and III the change of M_z is observed with a sign, opposite to ultrafast demagnetization. Based on it the authors concluded that the precession is triggered due to the partial suppression of the shape anisotropy orienting magnetization in the film plane.

Note, that the idea of magnetization precession excitation through ultrafast demagnetization and shape anisotropy suppression is very often used in MO pump-probe experiments, when the main interest is directly focused on the study of the magnetization precession of thin metallic films. Indeed, with that approach even a small demagnetization of about one percent is enough to excite precession with the frequency close to equilibrium value. This is why such method is an alternative for the ferromagnetic resonance (FMR). Furthermore, it provides spatial resolution of up to the units of micrometers.

It can be expected that the laser-induced heating of a magnetic material will also result in the modifications of the temperature-dependent parameters of magnetocrystalline, magnetoelastic and other types of single-ion anisotropy (see sect. 1.3). Thus, beginning from [46], a series of works
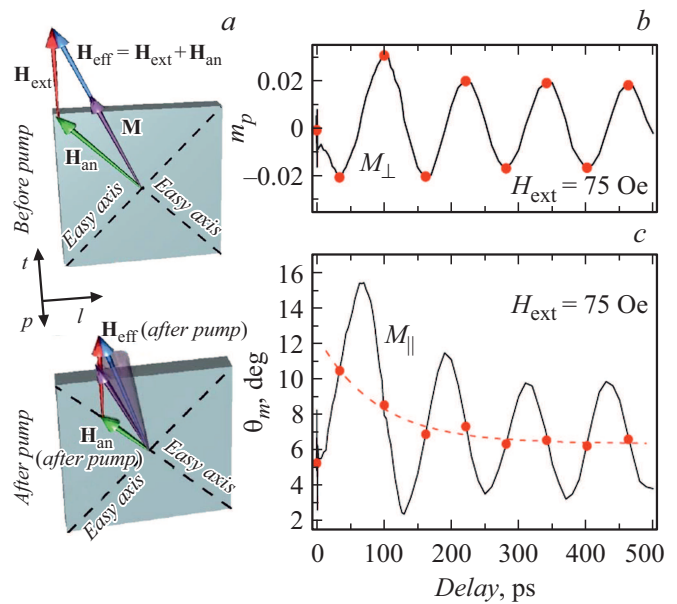

Figure 4. a — diagram showing orientation of magnetization $\mathbf{M}$ and effective field $\mathbf{H}_{eff} = \mathbf{H}_{ext} + \mathbf{H}_{an}$ in thin Fe/MgO(001) film in equilibrium (top) and immediately after excitation by laser pulse (bottom); b — magnetization projection normal to the film plane; c — in film plane along [100] crystallographic axis as a function of the delay time between the pump and probe pulses. The dashed line shows azimuthal angle of effective field $\mathbf{H}_{eff}$. $H_{ext} = 75$ Oe. (Figure is reproduced from [47].)

by various teams is devoted to the experimental study of the magnetization dynamics associated with the laser-induced modifications of the parameter K. One of the highly detailed studies from the point of view of methodology of laser-induced modifications of the magnetocrystalline anisotropy was performed in [38,47].

The work [47] studied the impact of laser pulses on 8 nm film of iron grown on the MgO (001) substrate. Iron possess cubical magnetocrystalline anisotropy with $K_1 > 0$ (1). Due to the orientation of the substrate and shape anisotropy, such film has two easy magnetization axes along the directions [100] and [010] laying in the film plane (Fig. 4, a). Fig. 4, a schematically shows the process of the magnetization precession launch as a result of ultrafast laser-induced heating with the further change of the parameter of magnetocrystalline anisotropy in the geometry, when external field is oriented at the angle of 45° to the axes of anisotropy. Experimental dependences of the magnetization polar angle proportional to the out of plane magnetization extension from the film plane, and the angle between magnetization and direction [100] in plane are shown in Fig. 4, b and c, respectively. Analysis of time dependences for various magnetization components allows to determine the evolution of the effective field direction and, hence, of the anisotropy field change. Thus, red dots in Fig. 4, b (in online version) show the maxima and minima of the magnetization polar angle. Since precession is

harmonic and effective field lays in the film plane, these dots correspond to the time, when the magnetization projection on the sample plane lays along the effective field $\mathbf{H}'_{\text{eff}}$. By marking the same time points on the dependence of the magnetization azimuthal angle in plane [47] we identified the changes in time of the effective field orientation (dashed line in Fig. 4, c). These changes match the fast (picosecond like) reduction of the value $H_A \sim K_1 M_S^{-1}$ and its further relaxation to the equilibrium on a timescale about hundreds of picoseconds.

The fact that laser-induced heating results in the reduction of the ratio $K_1 M_S^{-1}$ indicates that the anisotropy parameter K_1 changes stronger than the saturation magnetization M_S, analogously the case of equilibrium heating (see sect. 1.3). Moreover, the authors of [47] demonstrated that agreement between the changes of the anisotropy field and laser-induced increase of the lattice temperature with its further cooldown can be described by the model of temperature changes of the magnetic anisotropy parameter. In further works, using similar methods, several teams showed that in different ferromagnetic metals and metallic alloys the excitation by femtosecond laser pulses and heating result in the decrease of the parameters of magnetocrystalline [48,49], growth [49,50], magnetoelastic [51], and interface [29,52] anisotropy.

A number of studies paid special attention to confirming the validity of the relationship between changes of magnetization due to the laser-induced heating and the magnetic anisotropy parameters (6) at the time exceeding 10 ps, when the electron, spin and phonon subsystems of metal are in equilibrium [49,51]. However, the issue of the ratio between laser-induced changes of parameters of the single-ion magnetic anisotropy and saturation magnetization in metals during the first picoseconds after excitation, is still open.

3.1.2. Laser-induced heating in dielectrics

In magnetic dielectrics, in case of femtosecond laser pulse absorption, demagnetization is not ultrafast, but has characteristic times about a few hundreds of picoseconds [44,53]. Moreover, most of the time, the dielectrics saturation magnetization is considerably lower than in ferromagnetic metals. Therefore, the contribution of shape anisotropy to total magnetic anisotropy of dielectric is low, and its changes due to laser-induced demagnetization do not excite of magnetic dynamics with a significant amplitude.

In the absence of ultrafast demagnetization, laser-induced changes of magnetocrystalline and growth-induced anisotropy play a significant role in magnetization dynamics excitation in dielectrics. For example, in epitaxial monocrystalline films of practically relevant ferrimagnetic dielectrics — iron garnet with the general formula $M1_3(Fe,M2)_5O_{15}$, where M1 is yttrium, lanthanoid or rare-earth metal, M2 is gallium or aluminum, the growth-induced and associated with internal deformations anisotropy dominate and depend on a

series of factors, such as chemical composition of the film, mismatch on the film/substrate interface, and the growth conditions [54]. The cubic anisotropy in garnets usually is considerably lower than the growth-induced. Therefore, in iron garnet the required anisotropy can be tuned at the growth and post-growth stages, and the laser-induced heating allows to control it at short timescale.

A detailed study of laser-induced changes of the growth-induced anisotropy parameters due to the absorption of laser pulse and heating was performed in the work [53] for Bi-substituted iron garnet (Bi:YIG) grown on the substrate of gadolinium-gallium garnet (GGG) with orientation (210). Growth-induced magnetic anisotropy of such films has several contributions [54,55]:

$$W_A = K_u m_z^2 + K_i m_y^2 + K_{yz} m_y m_z, \qquad (8)$$

where K_u, K_i and K_{yz} are parameters of the uniaxial out-of-plane, uniaxial in-plane and orthorhombic components of anisotropy, respectively. The work [53] considers the excitation of the Bi:YIG by femtosecond laser pulses with photon energy in the range $1.65 - 2.0$ eV, where the Bi:YIG absorption coefficient changes from 300 to 750 cm^{-1}. As a result, the laser-induced magnetization precession amplitude increases when the pump pulse photon energy corresponds to more intensive absorption. These experiments demonstrated that the parameters of the growth anisotropy change as a result of laser-induced heating at timescale about a few picoseconds. According the estimates, heating at 10 K resulted in the change of the parameters ΔK about 1%.

In addition to the demonstration of the possibility of change of the parameters K due to laser-induced heating, the work [53] applied the method of separation of laser-induced changes of the parameters K, describing different types of anisotropy (8). Fig. 5, a shows the time dependence of the Faraday rotation for the probe pulses, proportional to the changes of the magnetization projection on the normal M_z film and measured for different directions of the external magnetic field $H_{\text{ext}} = 0.26$ T, applied in the film plane. In such a geometry of the experiment, the initial precession phase depends on the external field direction. It is determined by changes of the z-component of the torque $\mathbf{T}_0 = d\mathbf{M}dt^{-1}|_{\Delta t=0}$.

Its part derived from expressions (2), (7), (8), dependent on the laser-induced change of anisotropy parameters, has a form

$$\mathbf{T}_0 = \gamma \begin{pmatrix} 2(\Delta K_i - \Delta K_u)m_y m_z + \Delta K_{yz}(m_z^2 - m_y^2) \\ 2\Delta K_u m_x m_z + \Delta K_{yz} m_x m_y \\ 2\Delta K_i m_x m_y - \Delta K_{yz} m_x m_z \end{pmatrix}. \quad (9)$$

As can be seen from (9), the torque direction in case of laser pulse excitation is determined both by the ratio between the values of changes of different anisotropy parameters K, and by the initial direction of magnetization defined by equilibrium direction of the effective field of anisotropy $\mathbf{H}_A$ and external magnetic field $\mathbf{H}_{\text{ext}}$. Fig. 5, b
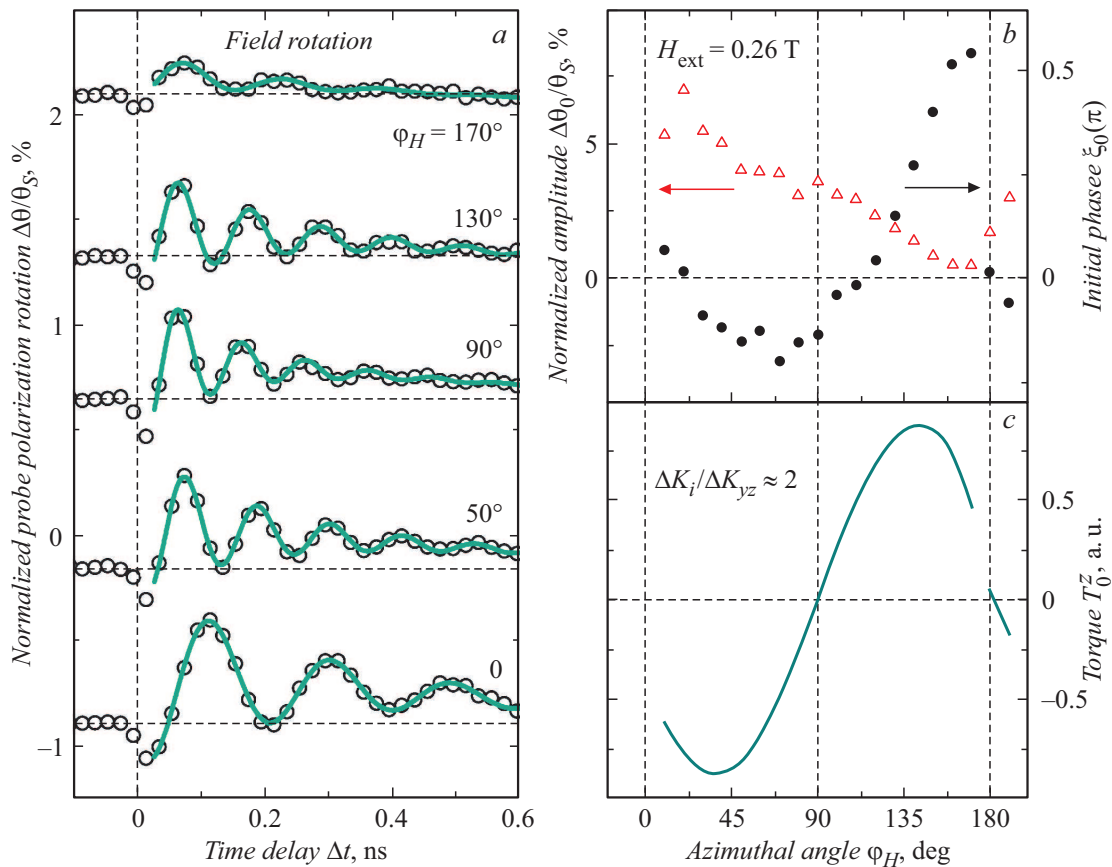
Figure 5. *a* — normalized rotation of probe pulses polarization plane, induced in the Bi:YIG/GGG(210) film by pump pulses, as a function of delay time Δt in the external field $H_{ext} = 0.26$ T, applied at different azimuthal angles φ_H; *b* — initial phase ξ_0 (solid symbols) and amplitude (normalized) $\Delta\theta_0/\theta_S$ (open symbols) of laser-induced oscillations of the normal component M_z as a function of φ_H; *c* — z-component of the spin-moment at the time of excitation $\Delta t = 0$ (9), calculated as the function of φ_H for the case when $\Delta K_i = 2\Delta K_{yz}$. (Figure is reproduced from [53].)

shows that the initial phase of precession significantly changes depending on the external magnetic field $\mathbf{H}_{ext}$ orientation. Calculation of the z-component of $\mathbf{T}_0$ as a function of azimuthal angle of the external field for the relative change of the parameters of the growth anisotropy $\Delta K_i = 2\Delta K_{yz}$ leads to a good agreement with the experimental data. Therefore, an analysis of the initial phase of precession allows to distinguish the laser-induced change of various parameters of magnetic anisotropy, even if they have similar time dependences.

Note, the fast laser-induced change of magnetic anisotropy parameters in dielectrics cannot be related to the slow laser-induced demagnetization [53]. Apparently, a decrease of the anisotropy parameters in a dielectric can be described by heat-induced increase of non-coherent optical and acoustic phonons disturbing crystal surrounding of magnetic ions. This results, in average, in loosening of the coupling between spin moments and the lattice. The work [53] demonstrated that at time delay ~ 500 ps, when the laser-induced demagnetization achieves its maximum, the ratio between changes of the anisotropy and magnetization satisfies (6).

Achievement of significant laser-induced changes of the parameters K in dielectrics requires the use of pulses with central energies of photon, corresponding to the high level absorption in green and blue regions of the optical spectrum. An alternative way of implementation of high anisotropy modification by laser-induced heating is possible in materials, where the competition between contributions of various nature to anisotropy results in its significant changes even at relatively low heating. An example of such materials is rare-earth orthoferrites $REFeO_3$ with temperature-induced spin-reorientation (SR) transitions occurs [25], when the anisotropy axis orientation is changed by 90° (see Fig. 1.3). Relatively low laser-induced heating $REFeO_3$ at the temperature a bit lower the SR transition is enough for the ultrafast transition detected by observing the magnetization precession around a new axis of anisotropy [56].

The SR transition in orthoferrites is determined by the temperature-dependent change of the magnetic moment RE^{3+}, i.e. the population of the ground state sublevels in the $4f$-shell RE^{3+} [26]. Thus, the laser-induced ultrafast excitation of $4f$-electrons must result in significant changes of magnetic anisotropy in rare-earth orthoferrites of a non-

thermal origin. However, the spectral width of femtosecond pulses is too broad versus the electron transitions in RE^{3+} ions, and absorption in visible and near infrared ranges is mainly determined by transitions in $3d$-shell of ions Fe^{3+}. Since the lifetime of excited $3d$-electrons is short, thermal equilibrium between them and the lattice takes place within a few hundreds of femtoseconds. The change of population of the $4f$-states of rare-earth ions occurs as a result of interaction with the lattice, and characteristic time of this process is determined by the electron-phonon interaction limiting the rate of the laser-induced SR transition to a few picoseconds [57].

3.2. Laser-induced dynamic and quasi-static strains

Ultrafast laser-induced heating in metals provides the feasibility of the magnetic anisotropy control by picosecond strains. This method uses approaches of picosecond acoustics developed in the 1980 s [58]. Generation of strain pulses with the duration about 10 ps occurs due to ultrafast expansion of crystal lattice under the effect of femtosecond laser pulse absorbed in a narrow surface layer of the excited structure [59]. The most common excitation scheme with the use of metallic film as an optoacoustic transducer is shown in Fig. 6, a. Bipolar strain pulse (see Fig. 6, b) propagates in a crystal at the speed of sound and is a wave packet of coherent acoustic phonons with the frequencies up to 100 GHz. Its amplitude depends on the density of optical excitation and may exceed 10^{-3}. The main mechanism determining the laser pulse energy conversion into coherent excitation of crystal lattice is optically-induced heating, but other mechanisms can also be involved, for example, deformation potential or piezoelectric one.

The feature of the first experiments on the ultrafast elastic control of magnetic anisotropy [60–62] was the generation of strain pulse in the substrate of the studied sample with further injection into film of a ferromagnet. The scheme of such experiment is shown in Fig. 6, c. The strain pulse injected into the film changes the value and direction of the magnetic anisotropy field, consequently, the direction of the effective magnetic field due to the inverse magnetostriction effect. The dynamic change of the energy of magnetic anisotropy is described by the formula (3), however, at the same time it has the spatial distribution varying in time and space during the strain pulse propagation within the magnetic layer.

However, in the majority of experiments with the films having thicknesses below 100 nm, the effect of magnetic anisotropy change can be described with a high accuracy by averaging the pulse-induced strain over the ferromagnetic film thickness. Precessional response of magnetization to such a ultrafast excitation allows to register changes of magnetic anisotropy and to determine its main parameters.

In the first experiments [60–62] performed according to the above mentioned method, epitaxial layers of the $(Ga, Mn)As$ ferromagnetic semiconductor were used. This
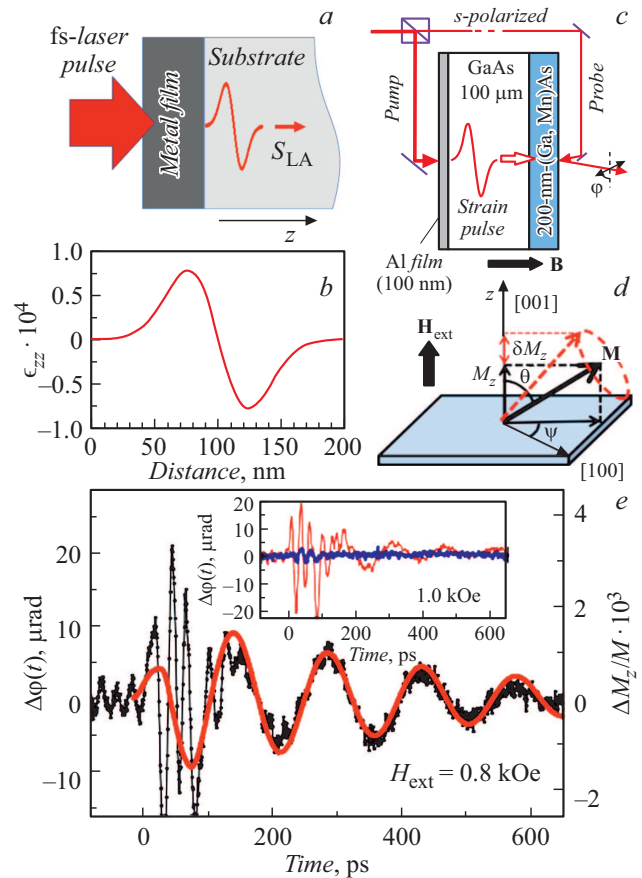

Figure 6. a — generation of picosecond strain pulse in case of femtosecond laser excitation of metallic film applied to a substrate of the studied structure; b — specific spatial profile of the strain pulse injected from a metallic film into the substrate. The pulse parameters match excitation of 100-nm aluminum film with the energy density of $1\,mJ/cm^2$. c — scheme of the first experiment for the modulation of magnetic anisotropy by laser-induced strain, performed in the geometry shown in panel (d); e — precession response of the $(Ga,Mn)As$ film magnetization to the modulation of magnetic anisotropy by the strain pulse [60]. The time $\Delta t = 0$ corresponds to the point when the strain pulse is reaching the $(Ga,Mn)As$ film. High-frequency oscillations observed in the signal (including those at $\Delta t < 0$) refer to manifestations of the elasto-optical effect. They are not associated with the magnetization modulation; their frequency does not depend on the magnetic field. However, the time interval $0 < \Delta t < 100\,ps$, where the elasto-optical modulation has the maximum amplitude, corresponds to the strain pulse propagation time in the $(Ga,Mn)As$ layer towards free surface and, after reflection, back towards the substrate. Red curve (in online version) refers to the result of numerical modeling of the magnetization response to spatial-time evolution of the magnetic anisotropy. Inset shows the outcome of control measurements with spatial misoverlap of the pump and probe pulses (blue curve (in online version)) resulting in a sharp drop of the amplitude of the measured kinetic signal, confirming coherent (non-thermal) behavior of the magnetic anisotropy modulation. (Figure is partially reproduced from [60] ($c-e$).)

material with cubic magnetocrystalline anisotropy features high magnetoelastic coefficients $B_1 = 25\,\mathrm{T}$, $B_2 = 150\,\mathrm{T}$ and low saturation magnetization $M_S \approx 10\,\mathrm{mT}$, which makes the deformation a dominating factor determining direction of the easy magnetization axes. In the scheme of the first experiment shown in Fig. 6, c, the external magnetic field was applied along the normal to the plane of the 200-nm thick $\mathrm{Ga_{0.95}Mn_{0.05}As}$ film. A change of the energy of magnetocrystalline anisotropy by the uniaxial strain pulse (the first element of the expression (3)) resulted in change of the effective field direction, consequently, in precession response of magnetization measured by the polar magnetooptical Kerr effect. Such experiment features considerably shorter time, when anisotropy differs from the equilibrium, in comparison with the experiments based on the ultrafast heating described above. This time is determined by the strain pulse duration and propagation time in a magnetic film.

Further experiments demonstrated the efficiency of uniaxial strain as a tool for the dynamic magnetic response excitation also with the in-plane application of external field in the $(\mathrm{Ga, Mn})\mathrm{As}$ films. In this case, a change of the effective magnetic field direction is determined by the modulation of the energy of magnetocrystalline anisotropy due to the higher order elements ($\sim B_3 m^4$). Though a low value of the magnetoelastic coefficient B_3 (effective field $0.5\,\mathrm{T}$) results in a low amplitude of modulation, nevertheless, this effect is detected in the experiment. Also, because of the presence of additional uniaxial anisotropy in plane of the $(\mathrm{Ga, Mn})\mathrm{As}$ films the dynamic strain-induced modulation of cubic anisotropy results in the change of direction of the effective magnetic field and excitation of precession even in zero external magnetic field. Further experiments with $(\mathrm{Ga, Mn})\mathrm{As}$ films grown on a low-symmetry substrates showed a high efficiency of the shear strain pulses, achieved due to a considerably higher value of the magnetoelastic coefficient B_2. A detailed theory of ultrafast modulation of magnetic anisotropy by strain pulses and the parameters of precession response of magnetization to such modulation was developed in the work [63].

The methods of ultrafast control of magnetic anisotropy by laser-induced strain pulses were also examined in the films of ferromagnetic metals of nickel [64] and galfenol $\mathrm{Fe_{81}Ga_{19}}$ [65] and in the ferrimagnetic dielectric yttrium-iron garnet [66]. The experiments with anisotropic films of nickel were carried out in the geometry with the external magnetic field oriented at an angle to the film plane, allowing to use non-zero projection of magnetization on the z axis for the modulation of magnetic anisotropy. In the galfenol films, as in the $(\mathrm{Ga,Mn})\mathrm{As}$, having a high cubic anisotropy, the precession response of magnetization is detected also in the magnetic field oriented in the film plane.

Taking into account the combination of characteristics: saturation magnetization up to $1.8\,\mathrm{T}$, Curie temperature up to $900\,\mathrm{K}$, strong magnetocrystalline anisotropy, high values of magnetoelastic coefficients ($B_1 = -6\,\mathrm{T}$, $B_2 = 2\,\mathrm{T}$) and

technological availability, for now, galfenol is the most promising material for applications in magnetic anisotropy control by means of laser-induced strain.

One of the branches of the development of this technique is the study of dynamic magnetoelastic effects in ferrimagnetic and ferromagnetic structures with pronounced elastic (phonon) resonances. In experiments with $\mathrm{FeBO_3}$ films with the thickness of a few microns [67] a femtosecond laser pulse excited elastic (phonon) eigenmodes of the ferrimagnetic film, quantized along the normal to the plane. The modulation of magnetocrystalline anisotropy induced by periodic strain with the frequency of up to $1\,\mathrm{GHz}$ (determined by the film thickness) manifested in driven oscillations of magnetization at this frequency and at higher harmonics.

Considerably higher frequencies (up to $35\,\mathrm{GHz}$) of the driven precession of magnetization were obtained in the experiments with galfenol films with the thickness $65\,\mathrm{nm}$ [68]. High Q-factor elastic eigenmodes there were formed using phonon Bragg mirrors — semiconductor superlattices arranged between the substrate and the ferromagnetic film. At the magnetic acoustic resonance condition, when the precession frequency controlled by the external magnetic field matched the phonon resonance, the magnetization oscillations amplitude demonstrated the sharp maximum. Resonance experiments were also carried out in nickel membranes [69] with spatially periodic optical excitation [70], in the structures with spatial periodicity in plane — 2D arrays of nickel nanomagnets [71] and galfenol-based ferromagnetic nanolattices [72,73], where surface phonon resonances are formed, as well as in single nanomagnets [74].

A common feature of experiments for the laser-induced modulation of magnetic anisotropy in the structure with high-Q elastic eigenmodes is not the pulsed, but the long-term effect of strain, periodically varying in time. The effects observed in such experiments, — magnetic acoustic resonance [68–74] and, when the strong coupling condition is achieved, formation of collective magnetoelastic excitation [73,74] — were also observed in classic magnetoacoustics [75]. However, the use of laser pulses for the generation of strain allows to implement them at considerably higher frequencies and nanometer scale.

It is important to know that in case of direct excitation by laser pulse of a thin film of a ferromagnetic metal, the strains occuring in it can be called quasi-stationary in the experiments on the laser-induced precession of magnetization. These strains are resulted from subpicosecond heating, and their quasi-stationary behavior is ensured by the fact that the metallic film cooldown process usually takes several microseconds exceeding by orders of magnitude typical period of magnetization precession. Until recently, such strains in the magnetic dynamics excitation and relaxation processes were not comprehensively studied. However, emergence of such quasi-static strain as a result of laser excitation leads to the emergence of additional terms in

the expression for magnetic part of free energy, associated with the inverse magnetostriction effect, and, in the general case, to the change of effective magnetic field affecting magnetization.

Experimental observation of the effect of such strain on the magnetization dynamics excitation is highly hindered by matching of the characteristic times describing the changes of the effective field due to quasi-static deformation and thermal change of the anisotropy parameters (see sect. 3.1). For distinguishing of two effects demonstrating similar temporal evolution, one must select experimental geometry, where the changes of the effective field $\mathbf{H}_{eff}$ orientation caused by such effects, would be different. In the work [50] this concept was implemented through the selection of a low-symmetry galfenol film grown on the GaAs substrate with orientation [311]. On the one hand, magnetocrystalline and growth-induced anisotropies make the axes of easy and hard magnetization lay in the film plane. In the experiment performed in the external magnetic field oriented along the axis of hard magnetization, laser-induced heating and reduction of the anisotropy parameters results in the change of the $\mathbf{H}_{eff}$ orientation in the film plane. On the other hand, laser-induced heating and film expansion resulted in the generation of quasi-static strains having quasi-longitudinal and quasi-transversal character (this process was reviewed in detail, for example, in [76]). An additional effective field $\mathbf{H}_{M-E}$ emerging due to the inverse magnetostriction effect, both changed the orientation of the total effective field in the plane, and resulted in its tilt from the film plane.

It was experimentally found that the trajectory of laser-induced precession varies depending on the value of the external magnetic field allowing to identify the direction of the effective field as a result of the laser excitation. It was shown that in external fields below the saturation, the direction of $\mathbf{H}_{eff}$ is affected both by the change of K, and quasi-stationary strains. With the increase of the external field above the saturation, the role of the laser-induced changes of K decreases, and the effect of quasi-stationary strains first of all the shear one persisted. The latter observation is a good illustration of the fundamental difference between laser-induced change of the parameters of magnetic anisotropy, but not its type, and the processes leading to emergence of new axes of magnetic anisotropy. The latter is interesting in terms of excitation of the magnetization precession in high magnetic fields, when the efficiency of the former considerably decreases. Note that identification of the role of laser-induced quasi-stationary strains in excitation of the magnetization dynamics was further developed in the work [77], where, in addition to the study of precession characteristics indicating the excitation mechanism, the authors measured directly the value and time profile of the laser-induced strain in a magnetic film using the Sagnac interferometry method with time resolution.

3.3. Ultrafast photomagnetic effects

The processes resulting in the change of the magnetic anisotropy type include an important class of the femtomagnetism phenomena — ultrafast photomagnetic effects. They are usually understood as laser-induced processes leading to the emergence of anisotropy axes not associated with heating. These phenomena are featured, generally, by pronounced dependence on the laser pulse photon energy and polarization. In terms of symmetry, the polarization-dependent laser-induced magnetic anisotropy is described by the introduction of the effective field

$$H_{LI,i} = \beta_{ijkl} E_j E_k^* M_l, \qquad (10)$$

where β_{ijkl} is the 4th order polar tensor, whose number of non-zero independent components is determined by the symmetry of the material, $\mathbf{E}$ is the light wave electrical field vector.

A good example of such phenomena are the processes observed in Co^{2+} substituted yittrium-iron garnets (Co:YIG) [78–80] and several other complex substituted garnets [81,82]. The feature of Co:YIG is to that a part of Fe^{3+} ions, in tetrahedral and octahedral positions, is substituted by Co^{2+} ions with unfrozen orbit moment. This results in a strong modification of the magnetic anisotropy value. Co:YIG with cubic anisotropy, in zero external magnetic field is divided into 90-degree domains. Earlier works on photoexcitation of Co:YIG showed the possibility to shift the 90-degree domain wall in case of excitation by linearly-polarized light with the wavelength 533 nm [83]. The domain wall shift towards one or another domain is determined by the laser pulse polarization, this implies that the observed effect is associated with the charge transfer between Co^{2+} ions in different positions. The charge transfer lead to the changes of magnetic anisotropy, described as the emergence of additional easy magnetization axis.

These works motivated the experiments with the excitation of Co:YIG films by linearly-polarized femtosecond laser pulses. The first experiments [78] on the Co:YIG films excitation by linearly-polarized pulses with the central wavelength of 800 nm, truly demonstrated the magnetization precession launch described by introducing an additional laser-induced axis of anisotropy, determined by the laser pulse polarization. Two key results were obtained in this work. First, it was found, that the effective field of the laser-induced anisotropy is enough for the observation of change of the magnetization precession period. It allowed to determine the effect relaxation time comparable with the magnetization precession period. Second, polarization dependence of the effect differs from observed in earlier works using longer laser pulses at the wavelength 533 nm. This observation indicated that, in different spectral ranges, the photomagnetic effect was determined by the excitations of Co^{2+} ions in different crystallographic positions. The development of studies of the photomagnetic phenomena

in Co:YIG further resulted in the implementation of a basically new method of spectrum- and polarization-dependent ultrafast recording of information discussed in sect. 4.1.3.

4. Applications and perspectives of the ultrafast control of magnetic anisotropy

As we discussed in the previous section, the ultrafast change of magnetic anisotropy results in the excitation of the magnetization precession, used in experiments to get information about the characteristics, timescales and absolute values of this process. However, ultrafast anisotropy change-induced precession of magnetization itself is prospective for different types of applications discussed in this section.

4.1. Precessional switching of magnetization

4.1.1. Switching by anisotropy suppression

One of the goals of the studies in the area of femtomagnetism is implementation of fast and efficient magnetization switching by single laser pulse [7,9,84]. On the other hand, precession switching of magnetization with the magnetic field and electric current pulses provides efficient and fast recording. This is why laser-induced changes of magnetic anisotropy being the precession triggers are now considered as a promising concept for the laser-induced information recording in magnetic materials.

In fact, if there are several magnetization orientations, corresponding to the minimum of free energy, for example, when the external constant magnetic field below the saturation is applied perpendicularly to the easy magnetization axis in uniaxial material. In this case there will be two minima of free energy, as shown in Fig. 1, e, and in case of ultrafast laser-induced suppression of magnetic anisotropy, magnetization precession is started. In case of sufficient precession amplitude and considerable damping, magnetization may relax into a position corresponding to the minimum of free energy different from the initial. Such a scenario for 90° magnetization switching was implemented in the iron film with the thickness of 8 nm grown on the MgO (001) substrate, where laser-induced heating results in the decrease of the cubic magnetocrystalline anisotropy (Fig. 4). The axes of magnetocrystalline anisotropy, between which switching was observed, are co-directional with crystallographic axes [100] and [010]. The external field was directed at the angle of 44° to [100], so the directions of [100] and [010] are non-equivalent, and in equilibrium position, magnetization is oriented almost longitudinally [100]. Fig. 7 shows two trajectories of laser-induced magnetic dynamics for the different values of the external field. In case of laser-induced excitation, the effective field of anisotropy $H_A \sim K_1 M_S^{-1}$ fastly decreases, followed by relaxation to the equilibrium value. Precession switching is controlled by the change of the external magnetic field altering the precession frequency. The balance between the precession period, damping time and the relaxation time of anisotropy field determines whether magnetization after a half of the period continues precession around the initial direction [100] or [010], what was observed in the experiment (Fig. 7, b and a respectively).

Implementation of such scenario of precession switching seems to be promising in materials, where magnetic anisotropy can be created locally at micron and submicron scales. An example of such structure is synthetic multiferroic — a ferromagnetic/ferroelectric heterostructure. The work [51] demonstrates the excitation by femtosecond laser pulses the CoFeB/BaTiO$_3$ multiferroic [16], consisting of 50 nm ferromagnetic amorphous metallic layer of Co$_{40}$Fe$_{40}$B$_{20}$ grown on the ferroelectric substrate BaTiO$_3$ (Fig. 8, a). At room temperature BaTiO$_3$ is divided into stripe 90° ferroelectric domains. Because of the strain transfer from the substrate to a magnetic layer, as well as of the inverse magnetostriction (see sect. 1.2), CoFeB is also divided into magnetic 90-degree domains characterized by uniaxial magnetoelastic anisotropy (Fig. 8, a). Its axes are oriented along the direction of spontaneous polarization in BaTiO$_3$ domains, since the magnetoelastic parameter CoFeB $B_1 < 0$. This material features the absence of magnetocrystalline contributions to magnetic anisotropy.

It was shown experimentally that in case of laser-induced heating, the magnetoelastic parameter and magnetization decrease ($\Delta B_1 \sim 27\%$, $\Delta M_S \sim 10\%$), resulting in excitation of the magnetization precession. Measurements of the ultrafast magnetic dynamics were performed in individual domains at different orientations of the external magnetic field relative to the anisotropy axes. Fig. 8, b shows experimental field dependences of the frequency and amplitude of precession in the experimental geometry, when the external field is oriented perpendicularly to the axis of anisotropy in a magnetic domain. The lines correspond to calculations based on the linearized solution of the LL equation. As we can see, the calculation curves for the precession frequency depending on the external field match the experimental data both quantitatively and qualitatively, meanwhile, there is a considerable disagreement, both quantitative and qualitative, for the amplitude. In case of excitation of the magnetization precession by anisotropy suppression, the precession amplitude maximum is achieved in the field, when the precession frequency is minimum. However, it is not observed in the experiment, and the amplitude maximum is shifted to the low fields. Therefore, within the range of fields, where precession of magnetization has the maximum amplitude, the amplitude of oscillations, detected in the experiment, of one of the magnetization projections was considerably suppressed.

Simulations of the laser-induced dynamics based on the LL equation (7) showed that around $H_{ext} = 50$ mT, the amplitude of excited precession is sufficient for the precession switching (Fig. 1, e). Depending on the relaxation time of the magnetization and magnetoelastic parameter B_1 to the equilibrium (Fig. 8, c, d) in the field $H_{ext} = 50$ mT, two scenarios of magnetization switching between two
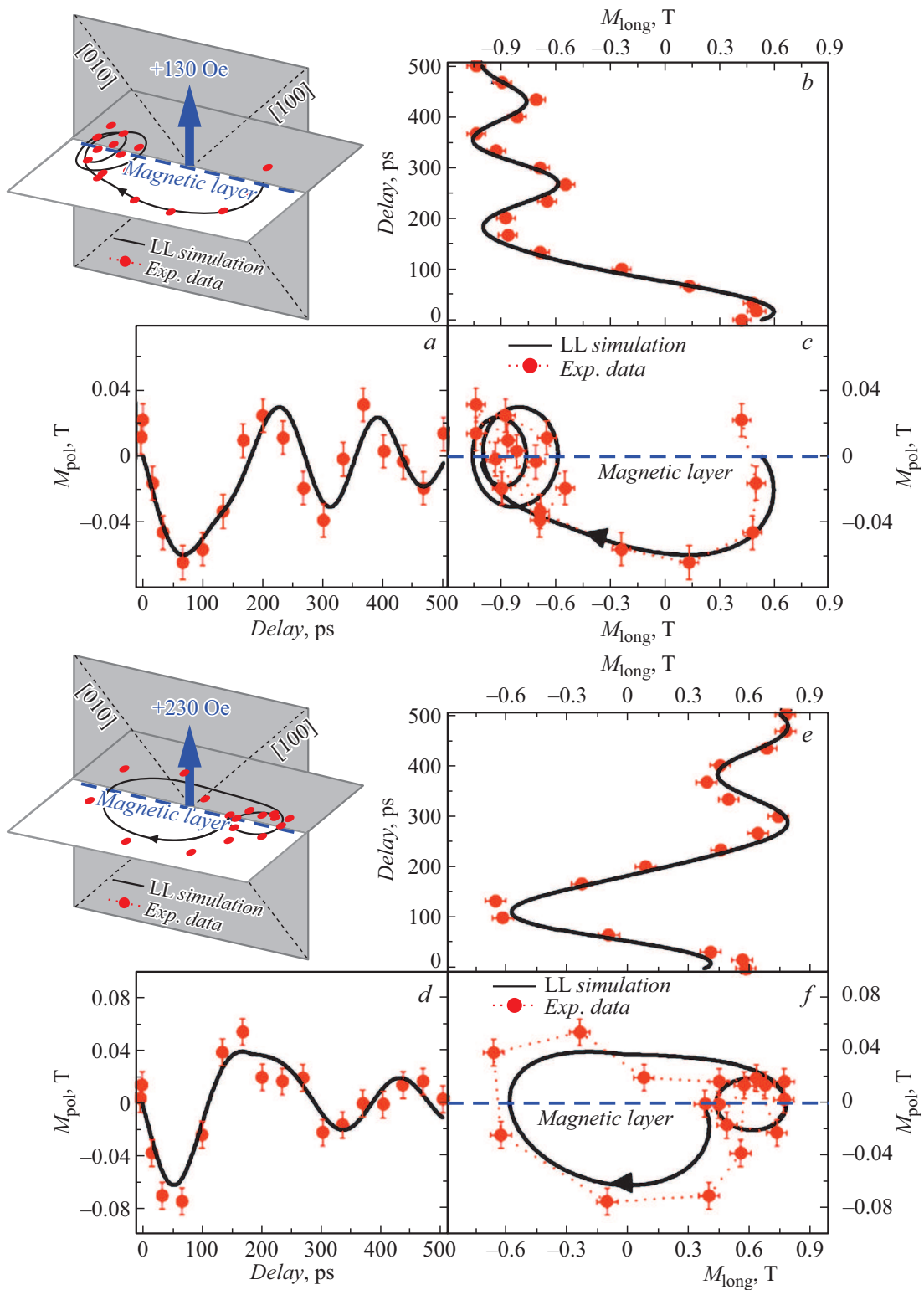
Figure 7. The Fe/MgO(001) film magnetization trajectory as a function of the delay time between the pump and probe pulses for two values of the external magnetic field $(a-c)$ $H_{ext} = 130$ Oe and $(d-f)$ $H_{ext} = 230$ Oe. Red dots (in online version) refer to experimental data, black lines are simulations based on the LL equation solution. Polar (a, d) and longitudinal (b, e) components were used for the reconstruction of the magnetization trajectory (c, f), projected on the surface normal to the magnetic field as shown in insets. (Figure is reproduced from [85].)
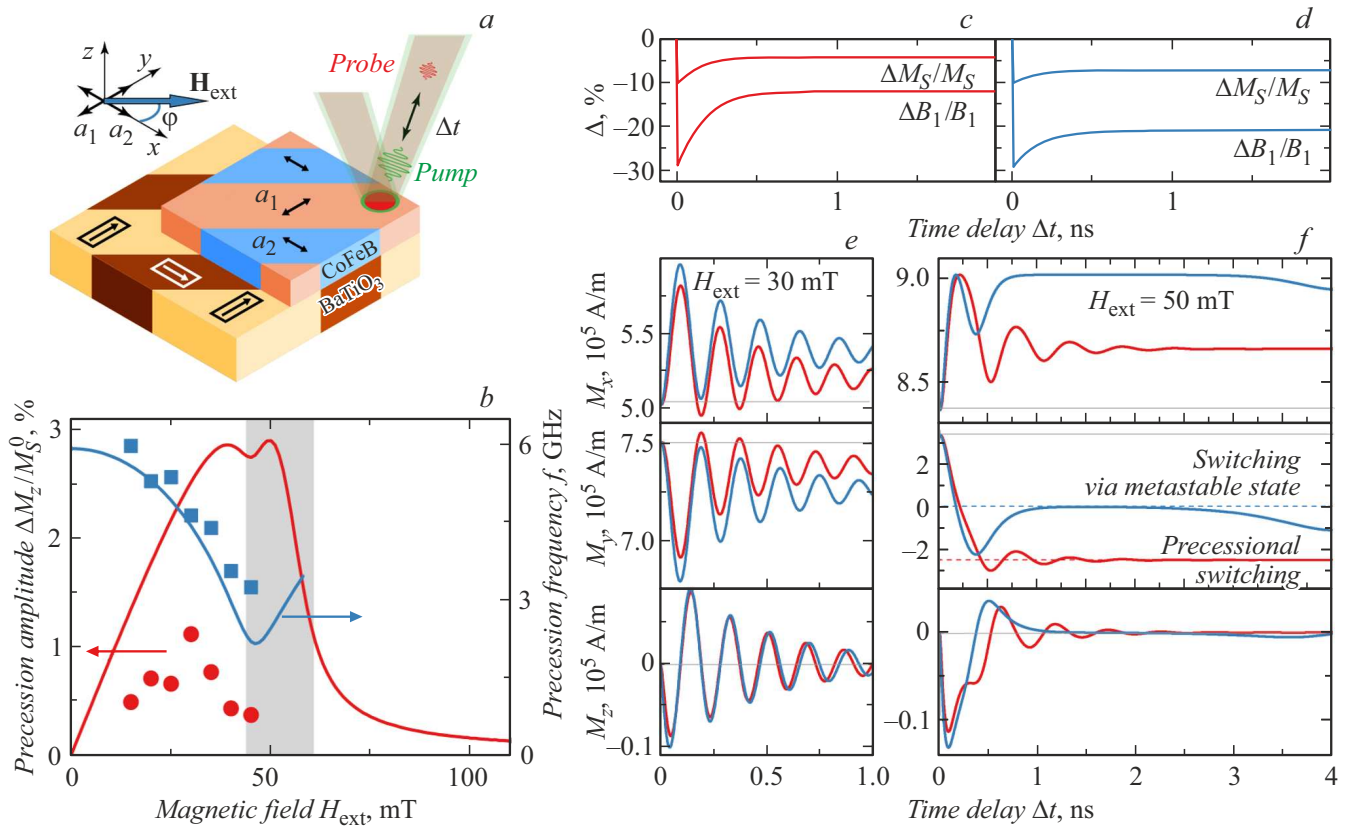
Figure 8. a — scheme of the experiment with laser-induced change of magnetoelastic anisotropy in synthetic multiferroic CoFeB/BaTiO$_3$. Different colors refer to 90° magnetic and ferroelectric domains; b — experimental dependences of the frequency f (blue squares (in online version)) and normalized amplitude $\Delta M_z^0/M_S$ (red circles (in online version)) precession of magnetization on the external magnetic field in the domain a_1, measured in the external field applied to the hard axis of magnetization in the domain a_1 at the angle $\varphi = -1°$. Solid lines are the calculation curves of the precession frequency and amplitude. c–f — simulation of laser-induced precession of magnetization, when the external magnetic field $\mathbf{H}_{ext}$ is applied along the hard magnetization axis (x). c,d — are evolutions of laser-induced changes of magnetization M_S and magnetoelastic parameter B_1, used in simulations, with different relaxation rates. e,f — dynamics of the magnetization components $M_{x,y,z}$ at $H_{ext} = 30$ mT (e) and $H_{ext} = 50$ mT (f). The results were obtained by using fast (red lines (in online version)) and slow (blue lines (in online version)) relaxation M_S and B_1, shown in panels (c and d), respectively. Grey lines show the equilibrium position of magnetization. Dashed red and blue lines (in online version) refer to switched and metastable conditions, respectively. (Figure is reproduced from [51].)

directions, corresponding to the minima of free energy, are realized (Fig. 8,f). In case of fast relaxation, the stable precession is achieved, otherwise — stochastic switching through metastable state. Around $H_{ext} = 30$ mT, the precession amplitude is lower and no switching occurs (Fig. 8,e). In the MO technique of pump-probe, assuming averaging over a large number of events, if magnetization is switched after every excitation by laser pulse, then the measured signal is close to zero, what is observed at $H_{ext} = 50$ mT. A reliable demonstration of switching in synthetic CoFeB/BaTiO$_3$ multiferroic and determination of the switching scenario details requires further experiments with single-pulse excitation and detection of the magnetization dynamics.

Precessional switching of magnetization in synthetic ferromagnet/piezoelectric multiferroics and magnetoelectrics attracts a lot of interest, since in such structures there

is a possibility to additionally control the orientation of anisotropy axes and the value of the anisotropy energy by applying electrical field to the ferroelectric or piezoelectric layer with high spatial resolution [17]. Moreover, in such structures there is a possibility to form a ferromagnetic layer with tuned properties, for example, the precession damping rate, being crucial for the precessional switching of magnetization, as shown in experiments with switching in iron garnet [86], discussed below.

Precessional switching of magnetization can be implemented in a dielectric as well, as was shown for the Bi:YIG film, epitaxially grown on the gadolinium-gallium garnet substrate with the orientation (111) [86]. In contrast with the work on precession excitation in the iron garnet film [53] discussed above, femtosecond laser pulses with the central photon energy of 3 eV, corresponding to the fundamental absorption in garnet, were used in order to
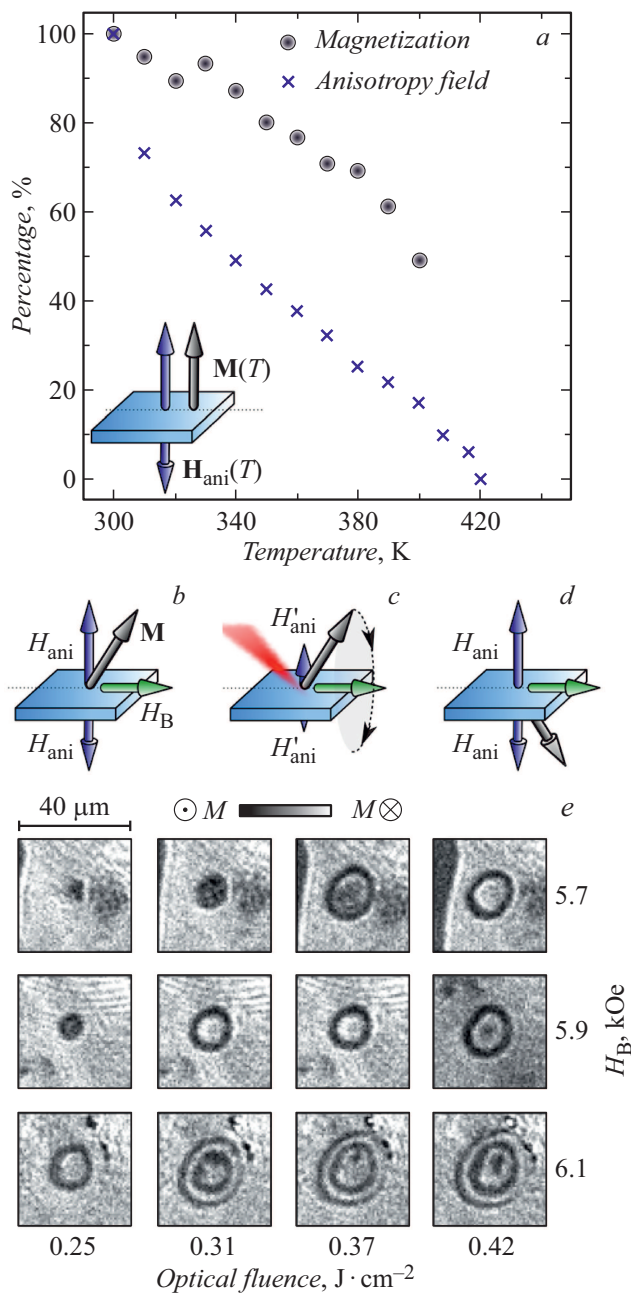
Figure 9. a — temperature dependence of equilibrium value of magnetization M (black circles) and field of perpendicular magnetic anisotropy H_{ani} (blue crosses (in online version)) of the Bi:YIG/GGG(111) film; b — in ground magnet state magnetization **M** lays along the effective field H_{eff}, consisting of the field of anisotropy H_{ami} and external field H_B oriented in the film plane; c — the anisotropy field temporarily decreases as a result of laser-induced heating, launching magnetization precession around new effective field, mainly defined by the external field H_B; d — after thermal energy dissipation, the anisotropy field returns to the equilibrium value fixing a new magnetization orientation; e — MO image of film taken 3.5 ns after excitation by single pump laser pulse, where dark regions with switched magnetization can be seen. The images were taken at the values of pump fluence and the external magnetic field oriented in the sample plane as shown in figure. (Figure is reproduced from [86].)

achieve significant suppression of the growth magnetic anisotropy and switching. Thus, ultrafast laser-induced heating was 30 K and resulted in the anisotropy field reduction by 45%. Such effect of femtosecond laser pulses led to the excitation of the magnetization precession with higher amplitude around the new position of the effective field, in this case mainly determined by the external field laying in the sample plane, as shown in Fig. 9, $b-d$. An important outcome also is the increase of the precession damping with the laser fluence. Because of that, when certain threshold fluence is achieved, a deterministic precession switching occurs, which was registered in magneto-optical images shot 3.5 ns after excitation by single laser pulse (Fig. 9, e). With the further increase of the pump fluence, precession becomes stochastic and then vanishes. It indicates that the Gilbert damping parameter α in this case is not a constant and is a function of time and amplitude of spatial distribution of the magnetic dynamics. It is important to note that such a temporary increase of damping is very high and contributes to magnetization switching to the other energy minimum. Therefore, [86] implemented more efficient approach to precessional switching of magnetization, requiring the precession damping time be comparable to a half of the precession period. If no such condition is met, then switching could not occur, since the magnetization relaxes to the initial state, as shown, for example, in the work with thin iron film (Fig. 7, f).

4.1.2. Switching by means of the spin-reorientation transition

The scenario discussed above for switching magnetization is implemented in the external magnetic field and in general case requires significant laser-induced increase of the temperature. These limitations are eliminated if switching is implemented by ultrafast laser-induced SR transition (see section 3.1). However, magnetization switching in case of ultrafast SR transition is stochastic because magnetization can be oriented in two opposite directions along the emerging axis of anisotropy equivalent in zero external magnetic field. To make controllable switching of magnetization through the ultrafast SR transition, it is necessary to additionally engage a special optomagnetic mechanism of interaction of laser pulses with magnetic materials [8].

Thus, the work [87] considered the excitation by single circularly polarized 60 fs laser pulses with the central photon energy 1.55 eV of the $(Sm,Pr)FeO_3$ bulk with the thickness 93 μm, cut perpendicularly to the crystallographic axis z. In the equilibrium state, at the temperature below $T_1 = 98$ K the system is at the minimum thermodynamic potential, and magnetization is oriented along the crystallographic axis x, which is the easy magnetization axis (Fig. 10, a, b). Femtosecond circular polarized laser pulse excites long-term precession of magnetization by means of the ultrafast inverse Faraday effect [88]. The amplitude of such precession, as a rule, is lower than $10°$, and its initial phase depends
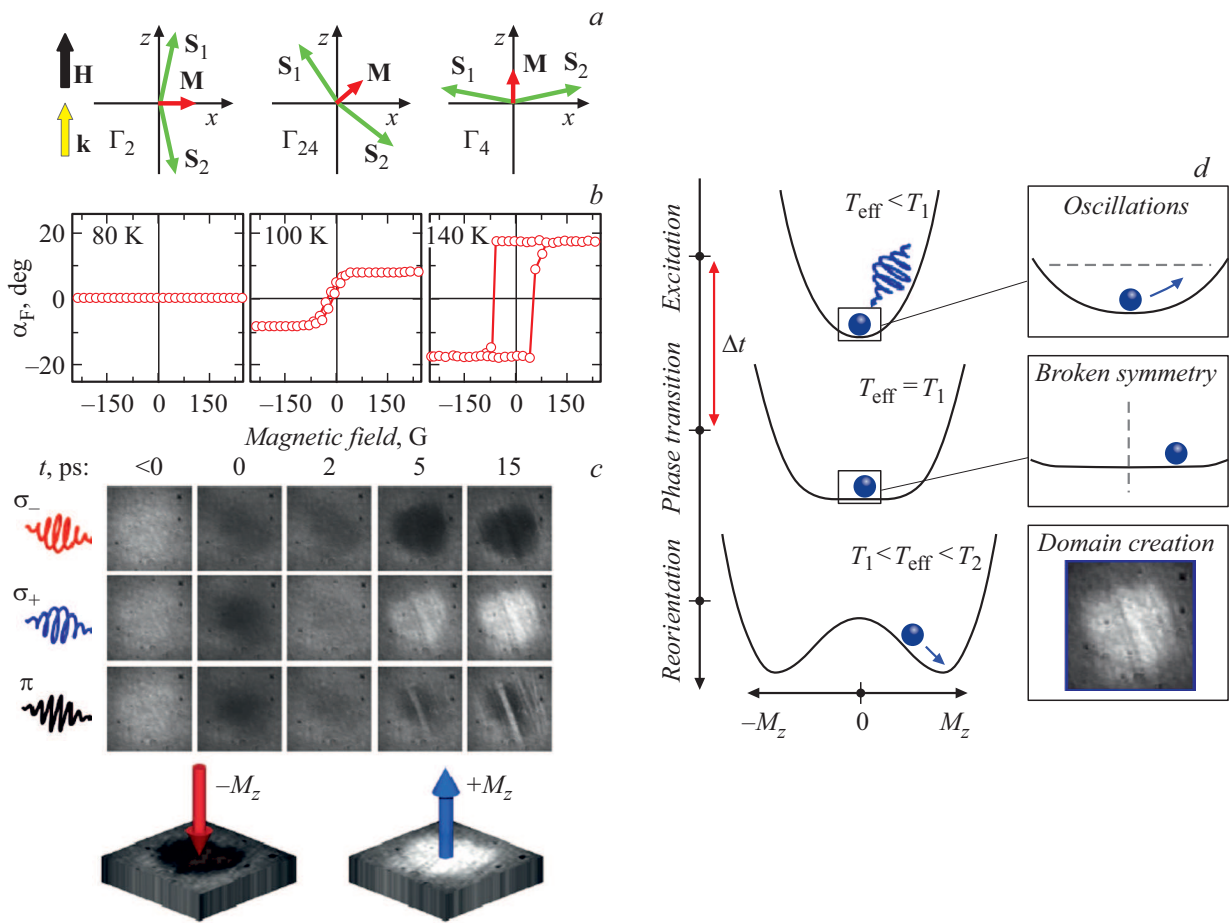
Figure 10. *a* — magnetic structure of rare earth orthoferrite $(Sm,Pt)FeO_3$ at the low temperature (Γ_2), in an intermediate phase Γ_{24} and in case of high temperature Γ_4; *b* — field dependences of z-component of a weak magnetic moment M in these phases. These measurements show the presence of two SR transitions leading to magnetic moment rotation $90°$ from the x axis to the z axis through the canted state; *c* — single-pulse MO image of a sample obtained at different delays after excitation by 60 fs laser pulse with the central wavelength 800 nm. Initial sample temperature — 90 K. Magnetic moment component out-of-plane is oriented either up (white color), or down (black color). It can be seen that laser pulses with different circular polarizations induce SR transition and emergence of the domain with opposite directions of the z-component of magnetization. Linearly polarized pulses create a multi-domain state. Size of images $\sim 70 \times 70\,\mu$m; *d* — illustration of the mechanism of control of laser-induced spin-reorientation transition through the dynamic symmetry breaking between two energy minima in high-temperature laser-induced phase (see text). (Figure is reproduced from [87].)

on the polarization of the exciting laser pulse. At the same time, laser pulse is partially absorbed and induces the second-order SR transition, when new anisotropy axis emerges several picoseconds after the excitation, and the profile of thermodynamic potential is changed (see sect. 3.1). Therefore, there are two simultaneous processes in the material. The first — precession of magnetization around the x axis with the period about 10 ps. The second includes gradual disappearing of the initial minimum and emergence of two new minima of the thermodynamic potential, corresponding to the orientation of magnetization along the z axis with different signs of the M_z component. Which one of the minima the magnetization will relax to, is determined by the initial precession phase, since it determines the proximity of M_z to one or another minimum, as well as by the number of half-periods in the time interval Δt between excitation and the emergence of new

minima of thermodynamic potential (Fig. 10, *d*). Therefore, with the initial temperature of the sample, exciting pulse fluence, as well as polarization of the pump pulses, one can control the switching of magnetization in rare earth orthoferrites [87].

Similar scenario of switching was also realized in $DyFeO_3$, between low temperature antiferromagnetic state and high temperature weak ferromagnetic, i.e. magnetization emergence was observed [89]. In $DyFeO_3$ the polarization dependence of the SR transition was always associated with another optomagnetic effect — the inverse Cotton-Mouton effect [90]. However, it should be noted, that ultrafast SR transition results in switching of magnetization between directions, stable at different temperatures. Therefore, switched state is preserved less than 1 ms, determined by the sample cooldown rate.

4.1.2.1. Photomagnetic switching

The use of the ultrafast photomagnetic effect discussed in sect. 3.3 for the implementation of precessional switching of magnetization fundamentally differs from the above considered methods, based on the change of the magnetic anisotropy parameters. Since the photomagnetic effect leads to the emergence of a new axis of anisotropy, switching between equilibrium states corresponding to the magnetization orientation along anisotropy axes in this case must be possible in zero field (Fig. 1,*f*). It was confirmed in [79] and further developed in [80,91].

Monocrystalline Co:YIG film on the GGG (001) substrate demonstrates a strong cubic anisotropy with easy axes $\langle 111 \rangle$. In [79], using single-pulse MO microscopy with femtosecond time resolution, authors demonstrated that the pulse linearly polarized along [100] with the central photon energy 0.95 eV induces the anisotropy axis along that direction with lifetime 20 ps. Therefore, if magnetization before laser pulse excitation is oriented along the easy axis close to [111], then the emergence of a laser-induced axis along [100] triggers the precession, which results in magnetization switching to [11$\bar{1}$]. Return of magnetization into the initial state is possible through the emergence of the anisotropy axis induced by laser pulse polarized along [010]. Having studied the magnetization dynamics in the process of switching, the authors [79] demonstrated that with a sufficient excitation pulse fluence, switching occurs within a fraction of the precession period. It is possible because of the balance between the precession period and lifetime of the induced axis of anisotropy, as well as a short time of the precession damping. Therefore, magnetization switching control in zero magnetic field was implemented changing the polarization of single laser pulses.

Further studies [80] performed using linearly polarized pulses with the central photon energy in the range $0.8-1.2$ eV, demonstrated that the observed switching has more degrees of freedom. Thus, switching between two cubic axes of anisotropy can be done also by the pulse polarized by [110] or [1$\bar{1}$0], if the photon energy is changed from 0.95 to 1.1 eV. This observation, first, enables the implementation of complex switching schemes between different axes using different combinations of laser pulses polarizations and the photon energies [80], inaccessible for the ultrafast heating. Second, this study explicitly showed that the emergence of one or another anisotropy axis is determined by the femtosecond laser pulse energy absorption in 3*d*-shell of Co^{2+} ions occupying tetrahedral (absorption at 0.95 eV) and octahedral (absorption at 1.1 eV) positions.

Note that the authors [79] called such magnetization switching „cold“ recording, in opposite to other concepts of magnetization switching, anyhow involving the heating and based on it. Search for other „cold“ mechanisms of magnetization switching requires identification of materials, where localized electron transitions may considerably affect magnetic anisotropy, as well as determination of spectral ranges of these transitions [92,93].

4.2. Ultrafast optomagnonics

Above, we discussed magnetic phenomena — precession and magnetization switching observed directly in the area of material affected by the laser pulse or laser-induced pulse of deformation. In this section, we review papers on the application of ultrafast change of magnetic anisotropy for the excitation of spin waves propagating in space, as well as on the impact on their parameters.

4.2.1. Optically reconfigurable magnonics

Today, alternatives to electronic devices for data processing and transmission at micro- and nanoscales include the elements of magnonics, where the transfer of magnetic moment in space occurs without charge transport due to the propagation of spin waves (SW) or coherent magnons in magnetically ordered structures [94,95]. The magnonics has numerous advantages over conventional electronics. One of these is the possibility of additional minimization of heat losses, as well as emergence of new degrees of freedom of processing of information associated with the wave properties of coherent magnons [96]. It is expected that the magnonics allows to solve a series of issues inherent to conventional electronics, such as ohmic losses, low frequencies, achieved limit of Moore's law, etc. Currently, active research is underway on the physical foundations for fast and efficient control of the spin-wave properties of magnonic elements, i.e. reconfigurable magnonic structures. The control concepts rely upon the sensitivity of magnetic parameters of materials, primarily, magnetization and magnetic anisotropy, to the external magnetic and electrical fields, temperature, mechanical stress, etc. [97]. By using one or a combination of these stimuli, one can modify the magnetic properties of structures and thus control a group and phase velocities of SW, direction of their propagation and other parameters.

One of the main challenges of creating reconfigurable magnonic structures is the provision of their fast switching (up to THz frequencies), high degree of localization of the excitation used for the reconfiguration of magnetic material's properties. A promising solution of that problem is the application of sub-picosecond dynamic processes initiated by the femtosecond laser pulses in magnetically ordered media.

The first works on control of the parameters of SW propagating in YIG films by optical pulses, appeared at the end of the last century [98–100]. Change of the YIG films magnetization in experiments occurred due to optical heating under the action of millisecond light pulses generated by a gas discharge lamp. As a result, the change of velocity, wave number and SW frequency was observed. The authors explained these effects based on the change of the SW dispersion in the case of reduction of magnetization, and, as a result, shape anisotropy of the YIG film. In a later
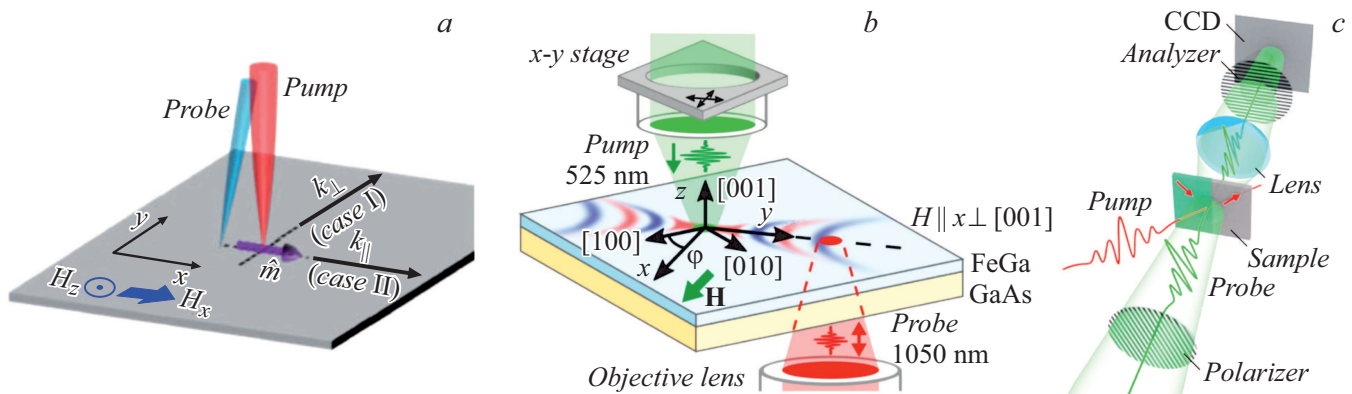
Figure 11. Schemes of implementation of 2D detection of optically excited spin waves: *a* — pump pulses and probe pulse are focused on the sample surface with microobjective or a lens; relative displacement of spots on the sample is provided by the change of the incidence angle of one of the pulses by a scanning mirror in front of the objective [110]; *b* — pump and probe pulses are focused on the sample surface from opposite sides with two different microobjectives; relative displacement of spots on the sample is provided by the displacement of one of the objectives [125]; *c* — use of CCD matrix to obtain the information on magnetization within a certain area of the sample at the same time [124]. (Figures are reproduced from [110] (*a*), [125] (*b*), [124] (*c*).)

work [101], optical heating of the YIG film was applied to create reconfigurable magnonic structures with a complexl geometry. The authors made spatially periodical heating of the magnonic wave guide with continuous laser radiation. It resulted in spatial modulation of local magnetization of the film, and, consequently, emergence of a magnonic crystal, whose band gaps' frequencies are determined by the distance between heated regions, with width is determined by laser intensity. A development of these studies led to the demonstration of activation/inactivation of magnonic lenses with the creation of the spatial gradient of laser-induced heating [102]. One more approach is the use of optical radiation for the modulation of the substrate properties, where magnetic medium is placed, thus changing the boundary conditions for propagating spin waves [103].

Regardless of the progress achieved in the area of optically reconfigurable magnonics, the issue of experimental implementation of the ultrafast dynamic reconfiguration of built-in elements and generation of induced magnonic elements, in fact, still remains open. From this perspective application of femtosecond phenomena for the local and ultrafast control of one or another characteristic of materials could solve the task.

4.2.2. Optical excitation of spin waves

The first application of femtomagnet phenomena concepts for the solution of the magnonics tasks, namely, generation of SW propagated in space by laser pulse, was realized in 2012. In a pioneer experimental work [104] by all-optical excitation and detection of SW with time and space resolution, the authors demonstrated that the application of optical pulses allows to control the initial parameters of SW. Thus, the change of the geometrical shape of the pump spot allows to control of the directional pattern of emitted SW through the change of the initial spectrum of excited wave

vectors. These results have initiated a series of studies of SW excited in different materials by laser pulses. In particular, application of optical techniques for all-optical excitation and detection of magnetostatic SW in metals was implemented in thin permalloy films [105–109], CoFeB [110] and Heusler compounds [111–113]. Excitation mechanism of this process is heat-induced ultrafast demagnetization (see sect. 3.1). However, most of the studies in this area are devoted to dielectrics — iron garnets substituted with bismuth Bi:YIG [114–124]. As a rule, for dielectric Bi:YIG films, excitation of SW occurs through inverse magneto-optical effects, what is out of scope this review. This is why further we discuss metallic films in detail where SW are excited as a result of ultrafast change of magnetocrystalline or shape anisotropy.

4.2.3. Experimental pump-probe technique with space resolution

For the observation of SW propagating along the magnetic film surface, the optical pump-probe technique described in sect. 2 must be modified. In particular, Besides to temporal evolution of the magnetization state, it is necessary to add the spatial scanning. There are three basic concepts of doing this given in Fig. 11:

1. The pump and probe pulses are focused on the sample surface with one microobjective or single lens; relative displacement of spots on the sample is achieved by the change of the incidence angle of one of the pulses by the scanning mirror in front of the focusing element;

2. The pump and probe pulses are focused on a magnetic film from the opposite sides with two different microobjective lenses; change of relative position of laser spots on the sample is provided by the displacement of one of the objectives;

3. Detection of the MO response is performed by CCD matrix to obtain the information on magnetization at the same time from a specific area of the sample lighted by probing pulses.

Methods 1 and 2 were successfully applied in experiments with metallic films. In experiments with Bi:YIG films, techniques 1 and 3 were used.

We also mention here the combined methods, when SW excitation occurs directly by AC magnetic field without the change in magnetic parameters of the material, and detection is implemented by optical methods — BLS or MO microscopy with time resolution [126,127]. In recent works [105,109] for the first time, resonance excitation of SW by fs laser with the pulse repetition rate of 1 GHz was combined with the waves' detection by BLS method.

4.2.4. Ultrafast change of magnetic anisotropy and excitation of spin waves

The ultrafast change of magnetic anisotropy results in the excitation of SW in metallic films and has not been experimentally demonstrated yet for Bi:YIG films and other dielectrics. The first experimental demonstration of the excitation of standing over the thickness SW was performed in the work [45] for films and structures made of nickel and permalloy. The change of magnetic shape anisotropy with ultrafast demagnetization was the physical mechanism initiating precession and SW (see sect. 1.3). Consequently, it is the optical change of the shape anisotropy that was used for the excitation of magnetostatic SW propagating along the film surface. Thus, asymmetric X-like propagation of SW pulses was observed in permalloy film by spatial scanning of the magnetooptical response [128]. Such X-shape is associated with anisotropy of SW dispersion relative to the external magnetic field direction. The change of in-plane component of magnetization results in the spatially asymmetric excitation of SW, meanwhile the film normal component determines asymmetric excitation. Since the presence of both components of the external magnetic fields is required for the excitation of SW through the change of shape anisotropy, the final picture of the SW propagation is neither fully symmetrical, nor antisymmetrical.

The work [128] stimulated the study of magnetostatic SW propagation in metallic films [105–113]. However, in all of these works, the exciting mechanism for SW is the change of shape anisotropy due to ultrafast demagnetization. It limits the experiment geometry by the need for magnetization tilt from the film's plane. This limit was overcome in the work [125], where the excitation mechanism is the ultrafast change of magnetocrystalline anisotropy. For the experiment, the authors used a 20 nm galfenol film ($Fe_{81}Ga_{19}$) with a strong cubic magnetocrystalline anisotropy and induced growth anisotropy of the easy axis type. Wherein, two axes of cubic anisotropy and the uniaxial anisotropy axis lay in the film's plane. It allowed exciting SW in the geometry when the external magnetic field is oriented parallel to the film plane (Fig. 12, a). Moreover the

presence of axes of anisotropy allowed to observe different velocities and lengths of the SW propagation for different mutual orientations of the external magnetic field and axes of magnetocrystalline anisotropy (Fig. 12, b). In addition, the narrowing of the SW spectrum was observed, when the wave propagates from the excitation region with the changed value of the anisotropy parameter into the region of undisturbed material. This was also observed earlier for in-plane isotropic films of permalloy [108], however, only to the region of low frequencies of the initially excited spectrum. The presence of in-plane magnetocrystalline anisotropy allowed to get such an effect also in the high-frequency region with the external magnetic field orientation along hard axis of anisotropy (Fig. 12, c, d). Dependence of the SW spectrum change behaviour in the presence of the spatial gradient of the magnetic anisotropy parameter is explained based on the SW dispersion [129].

Since the change of the magnetocrystalline anisotropy parameter by femtosecond laser pulse results in the local change of the SW dispersion, the area of light exposure can be considered as local inhomogeneity for the propagating SW [131,132]. In the work [130] it is suggested to use this feature for the formation of reconfigurable resonator for SW from optically pumped area and domain wall. Wherein the change of parameters of the laser pulse affects the parameters of one of the resonator mirrors, leading to the change of the spectra of the excited SW packet (Fig. 12, e). It should be noted that the presence of a domain wall or any other magnetic defect is a determinant factor for the SW excitation in considered system in zero external magnetic field. An interesting features of the system in the presence of a defect is that spatial position of the laser pulse determines the amplitude of the excited SW.

4.3. Localization of high-frequency magnetic excitations and fields at submicron scales

The most promising effects in terms of practical applications are caused by the interaction of localized elastic resonances and magnetization of the nanostructure. This is confirmed by a gradual transition occurred in studies of ultrafast optically induced magnetoelastic effects from injection of picosecond strain pulses with a wide spectrum in magnetic nanostructure to the experiments with direct optical excitation of magnetic nanostructures with high-Q elastic resonances.

The work [72] suggested using the effect of magnetoacoustic resonance at the frequencies ~ 10 GHz for the generation of AC magnetic fields with nanometer localization. In the experiment with nanolattices based on galfenol (Fig. 13, a) the laser pulse excites a localized surface elastic (phonon) mode. Under resonance conditions controlled by the external magnetic field (Fig. 13, b), the amplitude of magnetization precession at the frequency of crystal lattice exceeds 10^{-3} of the saturation magnetization. The field generated by precessing magnetization and localized in the
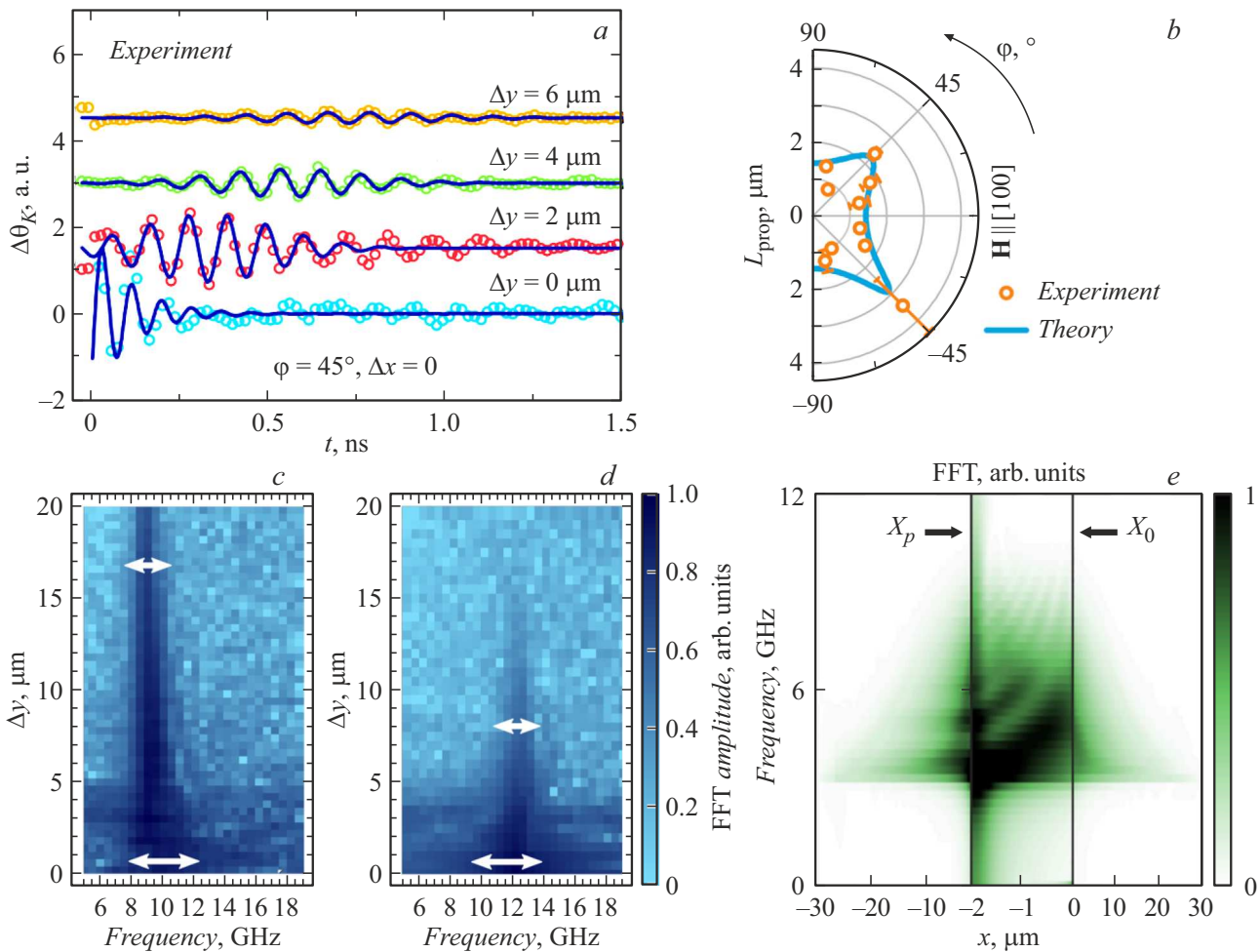
Figure 12. Pump-probe signals in case of optical excitation of the SW propagating in a thin FeGa/GaAs(100) galfenol film: a — time-resolved polar Kerr effect for different distances between the centers of pump and probe spots Δy; b — azimuthal dependence of the SW propagation length L_{prop}. In figures (a, b) symbols — experimental data, lines — theoretical calculation [125]. c, d — experimental spatial-spectral maps [129] illustrating the change of the spectra of the SW packet with distance from the excitation center with the external magnetic field orientation along the hard magnetization axis (c) and close to the easy magnetization axis (d). e — spatial-spectral map of the SW packet excited by laser pulse with the center x_p near to domain wall with the center at x_0 [130]. (Figures are reproduced from [125] (a, b), [129] (c, d), [130] (d, e).)

grooves of nanolattice reaches ~ 10 mT, exceeding the values achievable with stripe nanoantennas [133]. Similar effect of resonance pumping of the magnetization precession with optically excited localized phonon mode can be reached also in the structures with a more complex morphology, where nanometer localization of the generated magnetic field is reached in three directions. The results of such experiments are given in [134]. The suggested approach is an alternative for the use of nanooscillators excited by spin transfer torque. Practical applications, boosted by such technology include microwave-assisted magnetic recording [135] and magnetic resonance tomography with a nanometer resolution [136].

Another area, where the effects of resonance interaction of laser-induced deformation and magnetization in nanostructures can become widely applicable, refers to hybrid quantum magnonics [137]. Formation of hybridized excitation in the conditions of strong coupling of magnon

and phonon modes expands significantly the degrees of freedom for the manipulation of magnetic and elastic states. Until recently, observation of a strong magnon-phonon coupling in the experiments with femtosecond laser pulses seemed impossible. Significant limitations were imposed by the experimental method itself, meanwhile the generation of elastic and magnetic excitation with a wide spectrum and, consequently, their fast dephasing made the conditions for the observation of a strong coupling unfeasible. However, the use of structures with a complex design allowed to reach selective interaction only for a few optically-excited phonon and magnon modes out of a high number. As a result, manifestation of strong coupling and emergence of hybridized states excited by femtosecond laser pulses was demonstrated in nickel nanomagnets [74] and galfenol nanolattices [73].
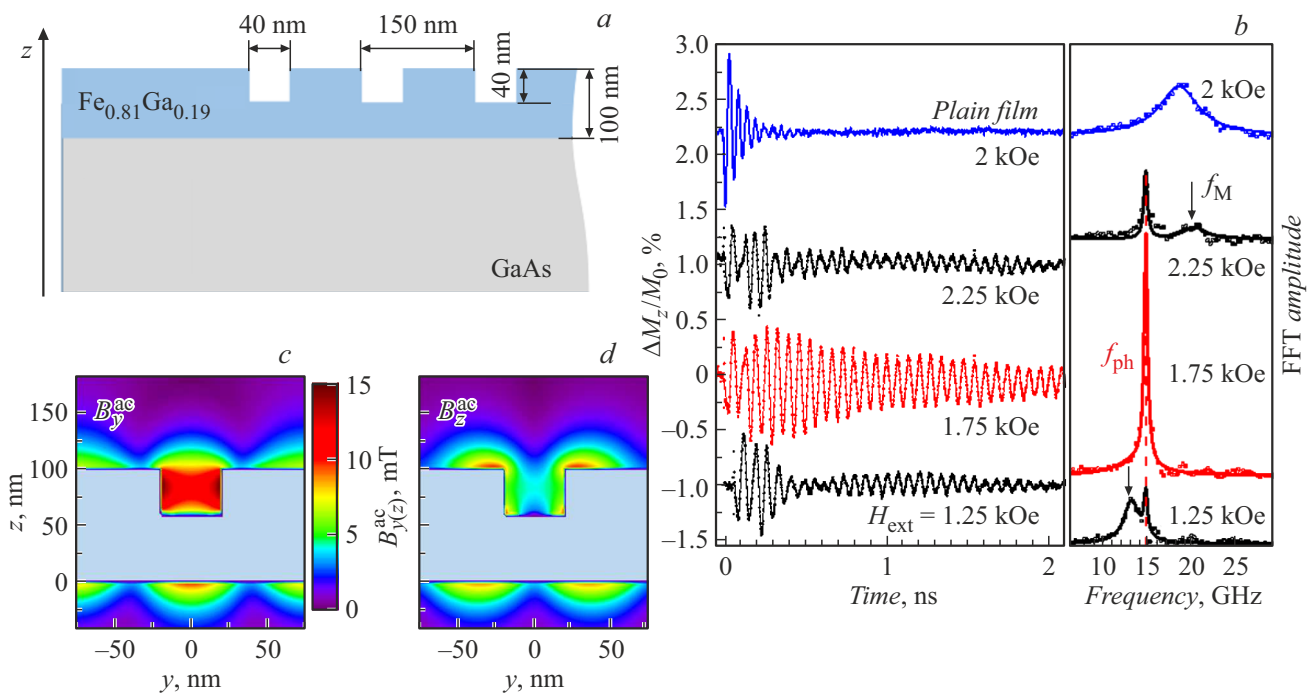
Figure 13. a — schematic image and main structural parameters of galfenol's nanolattice used in the experiment for the generation of a localized AC magnetic field by the resonance pumping of magnetization precession optically excited through surface phonon mode; b — precession response of magnetization measured by the polar magnetooptical Kerr effect (left panel) and its Fourier spectra (right panel) for direct optical excitation of a plain galfenol film (top curves) and nanolattice with three values of the external magnetic field. Black vertical arrows on the right panel show frequency of ferromagnetic resonance (f_M) with the relevant external magnetic field. Resonance pumping of precession in case of coincidence of FMR and superlattice phonon mode frequencies at $H_{ext} = 1.75$ mT is accompanied by a sharp increase of the spectral amplitude at resonance frequency $f_{ph} = 15$ GHz; c, d — spatial distributions of two orthogonal components of induction generated by precession magnetization of nanolattice [72]. (Figures reproduced from [72].)

4.4. Ultrafast laser-induced control of magnetic anisotropy beyond a research laboratory

Regardless of continuous development of the research methods for ultrafast magnetic effects by using femtosecond laser pulses and their great application potential, the need for the use of complex and large laser modules is a considerable limitation. To leave the laboratory optical table, a compact source of ultrashort laser pulses is needed. The solution is the technology of semiconductor mode-lock lasers (SMLL) [138]. A semiconductor laser radiation source with size $100\,\mu$m, is able to generate laser pulses with the duration below 1 ps at the repetition rate ~ 10 GHz and integral power up to 100 mW. The main application area of such laser systems in magnetic materials can be the resonance excitation of spin waves with optomagnetic effects. The resonance excitation of spin waves with a specified wave vector, as demonstrated in the experiments with classic laser systems [115], can be directly implemented with SMLL. The use of SMLL is also possible for the realization of elastic and temperature modulation of magnetic anisotropy.

A high repetition rate with low energy of a single pulse (~ 10 pJ), specific for SMLL, is not a limiting factor, regardless of small changes of the parameters of

the excited structure with the period considerably shorter than typical relaxation times. Recent experiments with metallic films demonstrated that the amplitude and duration of deformation pulses generated by SMLL is sufficient for direct optical detection [139]. Such pulses can be used for the ultrafast control of magnetic anisotropy. Recently performed experiments for optical excitation of galfenol films with the thickness of several nanometers by laser pulses with the repetition rate 10 GHz [140] showed that the temperature modulation at 0.1 K resulted in the excitation of quasi-stationary precession of magnetization, provided that the ferromagnetic resonance frequency controlled by the magnetic field matches the frequency of laser pulses repetition rate or its harmonics. The amplitude of not suppressed harmonic oscillations of magnetization in the resonance condition coincides with the precession amplitude achievable in the experiments with industrial laser amplifiers. Therefore, a combination of the SMLL technology and the methods of laser control of the nanostructures magnetic anisotropy can provide the implementation of as compact as possible (on-chip) devices of spin electronics with working principle based on all-optical control and readout of magnetic excitations.

Conclusion

The purpose of the review is to provide a reader a wide spectrum of phenomena occurring in magnetic materials under the excitation by femtosecond laser pulses of optical and near infrared ranges resulting in the ultrafast changes of various contributions into magnetic anisotropy. Among the best known phenomena there are effects associated with the ultrafast heating of magnetic material. As we demonstrated in the review, ultrafast heating efficiently suppresses the contributions to anisotropy, based on the spin-orbit interaction both in magnetic metals, and in dielectrics. In particular it relates to magnetocrystalline and magnetoelastic, and growth anisotropy.

After the excitation by femtosecond laser pulses, at the timescale of thermalization of electrons, lattice and spins, such changes of magnetic anisotropy are quite successfully described by the thermodynamic model connecting heating, magnetization reduction and parameters of magnetocrystalline anisotropy. However, the issue of correlation between laser-induced dynamics of magnetization and parameters of anisotropy at shorter timescales still remains open. In particular, in metals within the first picoseconds after excitation, electrons, lattice and spin subsystem are not in equilibrium. Evolution of parameters of magnetocrystalline anisotropy at these times is not studied, and it is not clear, whether it follows ultrafast changes of magnetization. Answering to this question is complicated, because the majority of studies of laser-induced anisotropy are based on the detection of the magnetization precession induced by such changes. Effective time resolution of such experiments is determined by the period of magnetization precession, i. e. tens of picoseconds in moderate magnetic field. Apparently, for the detailed study of laser-induced dynamics of magnetic anisotropy parameters during the first femto- and picoseconds after excitation by laser pulse, it is required to apply the techniques allowing to directly observe the changes of spin and orbit moments and interaction between them [141].

Magnetic metals have additional channel of the ultrafast suppression of magnetic anisotropy, related with ultrafast demagnetization. Due to this, in many experiments with ferromagnetic metals it is important to detect ultrafast changes of shape anisotropy of magnetodipole nature dominating in thin films and nanostructures. Moreover, in thin films and nanostructures magnetocrystalline and shape anisotropy coexist and the result is a balance between these two contributions. Such a situation provides perspectives for the implementation of a more complex response of magnetic anisotropy to ultrafast heating, because different contributions change differently with the same impact. It allows, for example, to implement laser-induced spin-reorientation transitions in metal-based nanostructures.

Such transitions have already been implemented in a series of magnetic dielectrics — rare earth orthoferrites, where the laser pulse excitation leading to the ultrafast heating change the balance between two contributions to magnetic anisotropy, causing the fast reorientation of the easy magnetization axis. Although in these experiments, the mechanism for changing the contributions to magnetic anisotropy was heating, it was necessary to repopulate the ground state sublevels of rare-earth ions. Therefore, the question of realization of magnetization switching by the ultrafast spin-reorientation transition in other iron oxides, such as magnetite, hematite, ferroborates, where no such channel of laser-induced change of anisotropy is presented, still remains open.

On the other hand, a determinant role of the electron state of rare-earth ion in the emergence of the ultrafast spin-reorientation transition gave rise to a new area in the studies of ultrafast changes of magnetic anisotropy, where instead of the non-resonant excitation of dielectrics leading to heating the selective excitation of certain electron transitions was realized. Such an excitation causes changes of spin-orbit or even exchange interactions determining magnetic anisotropy. For rare earth orthoferrites such transitions are in the infrared and even terahertz region, therefore, the experiments using exciting pulses in these spectral ranges, are promising. Significant progress in the area of excitation of magnetic dynamics by short pulses in these ranges, including change of the magnetic state and anisotropy of orthoferrites [92,142,143] can be the subject for a special review.

Note that the concept of resonant excitation of electron transitions due to the change of magnetic anisotropy can be realized also in the optical range [80,144], what is discussed in this review is shown by the example of cobalt substituted iron garnet. Of course, such approaches to anisotropy change have important benefits such as spectral selectivity and sensitivity to polarization of the exciting pulse. In addition to the resonant excitation of electron transitions, for anisotropy control one can also resonantly pump of phonon modes in the middle infrared range, what was demonstrated for rare earth $DyFeO_3$ orthoferrite, where phonon mode modulated the exchange contribution to anisotropy [144].

The change of magnetic anisotropy by laser-induced deformation has become another main line of research in this field. In addition to the direct anisotropy change in case of deformation in a material, these studies rely upon a key role of interactions between magnetic and elastic modes excited in magnetic nanostructures due to the ultrafast heating. Note, the interest appeared in this field to transition to the use of laser pulses beyond the optical range, allowing to directly excite phonon modes with further conversion into dynamic or quasi-static deformations [145]. Based on this approach the magnetization switching has already been implemented in iron garnet through deformations obtained by non-linear transformation of phonon modes excited in the middle infrared range [146].

The practically promising techniques can be implemented based on the mechanisms of magnetic anisotropy change reviewed herein. As part of the review, we elaborated on several approaches to implementing magnetization switching to record information, as well as to excite localized and

propagating magnon modes for magnonics and nanotomography.

Acknowledgments

The authors thank R.V. Pisarev, A.V. Kimel, A. Kirilyuk, Th. Rasing, D.R. Yakovlev, M. Bayer, A.V. Akimov, T.L. Linnik, A.W. Rushforth for many years of fruitful cooperation, as well as the team of the Ferroics Physics Laboratory of Ioffe Institute for useful discussions.

Funding

Conflict of interest

The authors declare that they have no conflict of interest.

References

[1] J. Michell. *A Treatise on Artificial Magnets* (Cambridge, 1750)

[2] J.P. Joule. Lond. Edinb. Dubl. Phil. Mag., **30**, 76 (1847).

[3] E. Villari. Il Nuovo Cimento (1855−1868), **20**, 317 (1865).

[4] C.S. Roumenin. *Solid State Magnetic Sensors* (Elsevier Science, London, 1994)

[5] B. Dieny, M. Chshiev. Rev. Mod. Phys., **89**, 025008 (2017).

[6] E. Beaurepaire, J.-C. Merle, A. Daunois, J.-Y. Bigot. Phys. Rev. Lett., **76**, 4250 (1996).

[7] A. Kirilyuk, A.V. Kimel, Th. Rasing. Rev. Mod. Phys., **82**, 2731 (2010).

[8] A.M. Kalashnikova, A.V. Kimel', R.V. Pisarev. UFN, **185** (10), 1064 (2015) (in Russian).

[9] A.V. Kimel, A.M. Kalashnikova, A. Pogrebna, A.K. Zvezdin. Phys. Reports, **852**, 1 (2020).

[10] A.G. Gurevich, G.A. Melkov. *Magnetization Oscillations and Waves* (CRC press, 1996)

[11] S. Tikazumi. *Ferromagnetism Physics. Magnetic properties of a substance* (Mir, Moscow, 1983)

[15] M. Tachiki. Prog. Theor. Exp. Phys., **23** (6), 1055 (1960).

[13] J.C. Slonczewski. J. Appl. Phys., **32** (3), S253 (1961).

[14] A.A. Bukharaev, A.K. Zvezdin, A.P. Pyatakov, Yu.K. Fetisov. UFN, **188** (12), 1288 (2018) (in Russian).

[15] J.-M. Hu, L.-Q. Chen, C.-W. Nan. Adv. Mater., **28** (1), 15 (2015).

[16] T.H.E. Lahtinen, J.O. Tuomi, S. van Dijken. Adv. Mater., **23** (28), 3187 (2013).

[17] R. LoConte, J. Gorchon, A. Mougin, C.H.A. Lambert, A. El-Ghazaly, A. Scholl, S. Salahuddin, J. Bokor. Phys. Rev. Mater., **2** (9), 091402 (2018).

[18] R.P. Cowburn, D.K. Koltsov, A.O. Adeyeye, M.E. Welland, D.M. Tricker. Phys. Rev. Lett., **83**, 1042 (1999).

[19] R.F.L. Evans, L. Rózsa, S. Jenkins, U. Atxitia. Phys. Rev. B, **102**, 020412 (2020).

[20] A. Fert, N. Reyren, V. Cros. Nat. Rev. Mater., **2** (7), 17031 (2017).

[21] J. Nogués, I.K. Schuller. J. Magn. Magn. Mater., **192** (2), 203 (1999).

[22] E.R. Callen, H.B. Callen. J. Phys. Chem. Solids, **16** (3), 310 (1960).

[23] C. Kittel, J.H. Van Vleck. Phys. Rev., **118**, 1231 (1960).

[24] E. Callen, H.B. Callen. Phys. Rev., **139**, A455 (1965).

[25] K.P. Belov, A.K. Zvezdin, A.M. Kadomtseva, R.Z. Levitin. UFN, **119** (7), 447 (1976) (in Russian).

[26] R.L. White. J. Appl. Phys., **40** (3), 1061 (1969).

[27] G. Malinowski, K.C. Kuiper, R. Lavrijsen, H.J.M. Swagten, B. Koopmans. Appl. Phys. Lett., **94** (10), 102501 (2009).

[28] S. Iihama, Q. Ma, T. Kubota, Sh. Mizukami, Y. Ando, T. Miyazaki. Appl. Phys. Express, **5** (8), 083001 (2012).

[29] J. Kisielewski, A. Kirilyuk, A. Stupakiewicz, A. Maziewski, A. Kimel, Th. Rasing, L.T. Baczewski, A. Wawro. Phys. Rev. B, **85**, 184429 (2012).

[30] V.F. Kovalenko, E.L. Nagaev. UFN, **148** (4), 561 (1986) (in Russian).

[31] M. Farle. Rep. Prog. Phys., **61** (7), 755 (1998).

[32] Th. Sebastian, K. Schultheiss, B. Obry, B. Hillebrands, H. Schultheiss. Front. Phys., **3**, 35 (2015).

[33] S. Foner. Versatile Rev. Sci. Instrum., **30** (7), 548 (1959).

[34] J. Clarke, A.I. Braginski. *The SQUID Handbook, Applications of SQUIDs and SQUID Systems* (John Wiley & Sons, 2006)

[35] A.K. Zvezdin, V.A. Kotov. *Modern Magnetooptics and Magnetooptical Materials* (CRC Press, 1997)

[36] L.D. Landau, E.M. Lifshitz. Phys. Z. Sowjetunion, **8**, 153 (1935).

[37] T.L. Gilbert. IEEE Trans. Magn., **40** (6), 3443 (2004).

[38] E. Carpene, E. Mancini, C. Dallera, E. Puppin, S. De Silvestri. J. Appl. Phys., **108** (6), 063919 (2010).

[39] J. Smit, H.G. Beljers. Philips Res. Repts, **10**, 113 (1955).

[40] H. Suhl. Phys. Rev., **97**, 555 (1955).

[41] B. Koopmans, G. Malinowski, F. Dalla Longa, D. Steiauf, M. Fähnle, T. Roth, M. Cinchetti, M. Aeschlimann. Nat. Mater., **9** (3), 259 (2010).

[42] M. Battiato, K. Carva, P.M. Oppeneer. Phys. Rev. Lett., **105**, 027203 (2010).

[43] K. Carva, P. Baláž, I. Radu. *Laser-Induced Ultrafast Magnetic Phenomena in Handbook of Magnetic Materials* (Elsevier B.V, 2017)

[44] A.V. Kimel, R.V. Pisarev, J. Hohlfeld, Th. Rasing. Phys. Rev. Lett., **89**, 287401 (2002).

[45] M. van Kampen, C. Jozsa, J.T. Kohlhepp, P. LeClair, L. Lagae, W.J.M. de Jonge, B. Koopmans. Phys. Rev. Lett., **88**, 227201 (2002).

[46] J.-Y. Bigot, M. Vomir, L.H.F. Andrade, E. Beaurepaire. Chem. Phys., **318** (1−2), 137 (2005).

[47] E. Carpene, E. Mancini, D. Dazzi, C. Dallera, E. Puppin, S. De Silvestri. Phys. Rev. B, **81**, 060415 (2010).

[48] J. Becker, O. Mosendz, D. Weller, A. Kirilyuk, J.C. Maan, P.C.M. Christianen, Th. Rasing, A. Kimel. Appl. Phys. Lett., **104** (15), 152412 (2014).

[49] P.I. Gerevenkov, D.V. Kuntu, Ia.A. Filatov, L.A. Shelukhin, M. Wang, D.P. Pattnaik, A.W. Rushforth, A.M. Kalashnikova, N.E. Khokhlov. Phys. Rev. Mater., **5**, 094407 (2021).

[50] V.N. Kats, T.L. Linnik, A.S. Salasyuk, A.W. Rushforth, M. Wang, P. Wadley, A.V. Akimov, S.A. Cavill, V. Holy, A.M. Kalashnikova, A.V. Scherbakov. Phys. Rev. B, **93**, 214422 (2016).

[51] L.A. Shelukhin, N.A. Pertsev, A.V. Scherbakov, D.L. Kazen-wadel, D.A. Kirilenko, S.J. Hämäläinen, S. van Dijken, A.M. Kalashnikova. Phys. Rev. Appl., **14**, 034061 (2020).

[52] B. Liu, L. Yang, X. Ruan, J.-W. Cai, L. He, H. Meng, J. Wu, Y. Xu. New J. Phys., **21** (5), 053032 (2019).

[53] L.A. Shelukhin, V.V. Pavlov, P.A. Usachev, P.Yu. Shamray, R.V. Pisarev, A.M. Kalashnikova. Phys. Rev. B, **97**, 014422 (2018).

[54] A.H. Eschenfelder. *Magnetic Bubble Technology. Springer Series in Solid-State Sciences 14* (Springer, Berlin, Heidelberg, 1980)

[55] I. Nistor, C. Holthaus, S. Tkachuk, I.D. Mayergoyz, C. Krafft. J. Appl. Phys., **101** (9), 09C526, 2007.

[56] A.V. Kimel, A. Kirilyuk, A. Tsvetkov, R.V. Pisarev, Th. Rasing. Nature, **429** (6994), 850 (2004).

[57] J.A. de Jong, A.V. Kimel, R.V. Pisarev, A. Kirilyuk, Th. Rasing. Phys. Rev. B, **84**, 104421 (2011).

[58] C. Thomsen, H.T. Grahn, H.J. Maris, J. Tauc. Phys. Rev. B, **34**, 4129 (1986).

[59] O. Matsuda, M.C. Larciprete, R.L. Voti, O.B. Wright. Ultrasonics, **56**, 3 (2015).

[60] A.V. Scherbakov, A.S. Salasyuk, A.V. Akimov, X. Liu, M. Bombeck, C. Brüggemann, D.R. Yakovlev, V.F. Sapega, J.K. Furdyna, M. Bayer. Phys. Rev. Lett., **105**, 117204 (2010).

[61] M. Bombeck, A.S. Salasyuk, B.A. Glavin, A.V. Scherbakov, C. Brüggemann, D.R. Yakovlev, V.F. Sapega, X. Liu, J.K. Furdyna, A.V. Akimov, M. Bayer. Phys. Rev. B, **85**, 195324 (2012).

[62] M. Bombeck, J.V. Jäger, A.V. Scherbakov, T. Linnik, D.R. Yakovlev, X. Liu, J.K. Furdyna, A.V. Akimov, M. Bayer. Phys. Rev. B, **87**, 060302(R) (2013).

[63] T.L. Linnik, A.V. Scherbakov, D.R. Yakovlev, X. Liu, J.K. Furdyna, M. Bayer. Phys. Rev. B, **84**, 214432 (2011).

[64] J.-W. Kim, M. Vomir, J.-Y. Bigot. Phys. Rev. Lett., **109** (16), 166601 (2012).

[65] J.V. Jäger, A.V. Scherbakov, T.L. Linnik, D.R. Yakovlev, M. Wang, P. Wadley, V. Holy, S.A. Cavill, A.V. Akimov, A.W. Rushforth, M. Bayer. Appl. Phys. Lett., **103** (3), 032409 (2013).

[66] M. Deb, E. Popova, M. Hehn, N. Keller, S. Mangin, G. Malinowski. Phys. Rev. B, **98** (17), 174407 (2018).

[67] D. Afanasiev, I. Razdolski, K.M. Skibinsky, D. Bolotin, S.V. Yagupov, M.B. Strugatsky, A. Kirilyuk, Th. Rasing, A.V. Kimel. Phys. Rev. Lett., **112**, 147403 (2014).

[68] J.V. Jäger, A.V. Scherbakov, B.A. Glavin, A.S. Salasyuk, R.P. Campion, A.W. Rushforth, D.R. Yakovlev, A.V. Akimov, M. Bayer. Phys. Rev. B, **92**, 020404(R) (2015).

[69] J.-W. Kim, J.-Y. Bigot. Phys. Rev. B, **95**, 144422 (2017).

[70] J. Janušonis, C.L. Chang, P.H.M. van Loosdrecht, R.I. Tobey. Appl. Phys. Lett., **106** (18), 181601 (2015).

[71] Y. Yahagi, B. Harteneck, S. Cabrini, H. Schmidt. Phys. Rev. B, **90**, 140405 (2014).

[72] A.S. Salasyuk, A.V. Rudkovskaya, A.P. Danilov, B.A. Glavin, S.M. Kukhtaruk, M. Wang, A.W. Rushforth, P.A. Nekludova, S.V. Sokolov, A.A. Elistratov, D.R. Yakovlev, M. Bayer, A.V. Akimov, A.V. Scherbakov. Phys. Rev. B, **97**, 060404 (2018).

[73] F. Godejohann, A.V. Scherbakov, S.M. Kukhtaruk, A.N. Poddubny, D.D. Yaremkevich, M. Wang, A. Nadzeyka, D.R. Yakovlev, A.W. Rushforth, A.V. Akimov, M. Bayer. Phys. Rev. B, **102**, 144438 (2020).

[74] C. Berk, M. Jaris, W. Yang, S. Dhuey, S. Cabrini, H. Schmidt. Nat. Commun., **10**, Art. Num. 2652 (2019).

[75] O.Yu. Belyaeva, L.K. Zarembo, S.N. Karpachev. UFN, **162** (2), 107 (1992) (in Russian).

[76] T.L. Linnik, V.N. Kats, J. Jäger, A.S. Salasyuk, D.R. Yakovlev, A.W. Rushforth, A.V. Akimov, A.M. Kalashnikova, M. Bayer, A.V. Scherbakov. Phys. Scr., **92** (5), 054006 (2017).

[77] Y. Shin, M. Vomir, D.-H. Kim, P.C. Van, J.-R. Jeong, J.-W. Kim. ArXiv, 2105.04168, 2021.

[78] F. Atoneche, A.M. Kalashnikova, A.V. Kimel, A. Stupakiewicz, A. Maziewski, A. Kirilyuk, Th. Rasing. Phys. Rev. B, **81**, 214440 (2010).

[79] A. Stupakiewicz, K. Szerenos, D. Afanasiev, A. Kirilyuk, A.V. Kimel. Nature, **542** (7639), 71 (2017).

[80] A. Stupakiewicz, K. Szerenos, M.D. Davydova, K.A. Zvezdin, A.K. Zvezdin, A. Kirilyuk, A.V. Kimel. Nat. Commun., **10**, 612 (2019).

[81] F. Hansteen, A. Kimel, A. Kirilyuk, Th. Rasing. Phys. Rev. Lett., **95**, 047402 (2005).

[82] F. Hansteen, A.V. Kimel, A. Kirilyuk, Th. Rasing. Phys. Rev. B, **73**, 014421 (2006).

[83] A. Stupakiewicz, A. Maziewski, I. Davidenko, V. Zablotskii. Phys. Rev. B, **64**, 064405 (2001).

[84] A.V. Kimel, M. Li. Nat. Rev. Mater., **4** (3), 189 (2019).

[85] E. Carpene, C. Piovera, C. Dallera, E. Mancini, E. Puppin. Phys. Rev. B, **84**, 134425 (2011).

[86] C.S. Davies, K.H. Prabhakara, M.D. Davydova, K.A. Zvezdin, T.B. Shapaeva, S. Wang, A.K. Zvezdin, A. Kirilyuk, Th. Rasing, A.V. Kimel. Phys. Rev. Lett., **122**, 027202 (2019).

[87] J.A. de Jong, I. Razdolski, A.M. Kalashnikova, R.V. Pisarev, A.M. Balbashov, A. Kirilyuk, Th. Rasing, A.V. Kimel. Phys. Rev. Lett., **108**, 157601 (2012).

[88] A.V. Kimel, A. Kirilyuk, P.A. Usachev, R.V. Pisarev, A.M. Balbashov, Th. Rasing. Nature, **435** (7042), 655 (2005).

[89] D. Afanasiev, B.A. Ivanov, A. Kirilyuk, Th. Rasing, R.V. Pisarev, A.V. Kimel. Phys. Rev. Lett., **116**, 097401 (2016).

[90] A.M. Kalashnikova, A.V. Kimel, R.V. Pisarev, V.N. Gridnev, A. Kirilyuk, Th. Rasing. Phys. Rev. Lett., **99**, 167205 (2007).

[91] A. Frej, A. Maziewski, A. Stupakiewicz. Appl. Phys. Lett., **118** (26), 262401 (2021).

[92] R.V. Mikhaylovskiy, T.J. Huisman, R.V. Pisarev, Th. Rasing, A.V. Kimel. Phys. Rev. Lett., **118**, 017205 (2017).

[93] D. Afanasiev, J.R. Hortensius, M. Matthiesen, S. Mañas-Valero, M. Šiškins, M. Lee, E. Lesne, H.S.J. van der Zant, P.G. Steeneken, B.A. Ivanov, E. Coronado, A.D. Caviglia. Sci. Adv., **7**, 23 (2021).

[94] S.A. Nikitov, D.V. Kalyabin, I.V. Lisenkov, A.N. Slavin, Yu.N. Barabanenkov, S.A. Osokin, A.V. Sadovnikov, E.N. Beginin, M.A. Morozova, Yu.P. Sharaevskiy, Yu.A. Filimonov, Yu.V. Khivintsev, S.L. Vysotsky, V.K. Sakharov, E.S. Pavlov. UFN, **185** (10), 1099 (2015) (in Russian).

[95] S.A. Nikitov, A.R. Safin, D.V. Kalyabin, A.V. Sadovnikov, E.N. Beginin, M.V. Logunov, M.A. Morozova, S.A. Odintsov, S.A. Osokin, A.Yu. Sharaevskaya, Yu.P. Sharaevskiy, A.I. Kirilyuk. UFN, **190** (10), 1009 (2020) (in Russian).

[96] A. Mahmoud, F. Ciubotaru, F. Vanderveken, A.V. Chumak, S. Hamdioui, C. Adelmann, S. Cotofana. J. Appl. Phys., **128** (16), 161101 (2020).

[97] D. Grundler. Nature Phys, **11** (6), 438 (2015).

[98] Y.K. Fetisov, I.V. Romanov, V.B. Studenov. Electron. Lett., **31** (14), 1168 (1995).

[99] S.N. Dunaev, Y.K. Fetisov. IEEE Trans. Magn., **31** (6), 3488 (1995).

[100] Y.K. Fetisov, A.V. Makovkin. J. Appl. Phys., **79** (8), 5721 (1996).

[101] M. Vogel, A.V. Chumak, E.H. Waller, T. Langner, V.I. Vasyuchka, B. Hillebrands, G. Von Freymann. Nat. Phys., **11** (6), 487 (2015).

[102] M. Vogel, R. Aßmann, P. Pirro, A.V. Chumak, B. Hillebrands, G. von Freymann. Sci. Rep., **8**, 11099 (2018).

[103] A.V. Sadovnikov, E.N. Beginin, S.E. Sheshukova, Yu.P. Sharaevskii, A.I. Stognij, N.N. Novitski, V.K. Sakharov, Yu.V. Khivintsev, S.A. Nikitov. Phys. Rev. B, **99**, 054424 (2019).

[104] T. Satoh, Y. Terui, R. Moriya, B.A. Ivanov, K. Ando, E. Saitoh, T. Shimura, K. Kuroda. Nat. Photonics, **6** (10), 662 (2012).

[105] S. Muralidhar, R. Khymyn, A.A. Awad, A. Alemán, D. Hanstorp, J. Åkerman. Phys. Rev. Lett., **126**, 037204 (2021).

[106] S. Iihama, Y. Sasaki, A. Sugihara, A. Kamimaki, Y. Ando, S. Mizukami. Phys. Rev. B, **94**, 020401 (2016).

[107] A. Kamimaki, S. Iihama, Y. Sasaki, Y. Ando, S. Mizukami. Phys. Rev. B, **96**, 014438 (2017).

[108] A. Kamimaki, S. Iihama, Y. Sasaki, Y. Ando, S. Mizukami. IEEE Trans. Magn., **53** (11), 1 (2017).

[109] S. Muralidhar, A.A. Awad, A. Alemán, R. Khymyn, M. Dvornik, D. Hanstorp, J. Åkerman. Phys. Rev. B, **101**, 224423 (2020).

[110] S.-J. Yun, C.-G. Cho, S.-B. Choe. Appl. Phys. Express, **8** (6), 063009 (2015).

[111] Z. Chen, Y. Yan, S. Li, X. Xu, Y. Jiang, T. Lai. Sci. Rep., **7**, 42513 (2017).

[112] Z. Chen, Z. Xie, S. Li, J. Zhou, W. Zhang, C. Zhang, J. Peng, J. Chen, B. Zhang. Appl. Phys., **127** (23), 233903 (2020).

[113] S. Li, C. Cheng, K. Meng, C. Chen. Jpn. J. Appl. Phys., **58** (4), 040903 (2019).

[114] A.I. Chernov, M.A. Kozhaev, I.V. Savochkin, D.V. Dodonov, P.M. Vetoshko, A.K. Zvezdin, V.I. Belotelov. Opt. Lett., **42** (2), 279 (2017).

[115] M. Jäckl, V.I. Belotelov, I.A. Akimov, I.V. Savochkin, D.R. Yakovlev, A.K. Zvezdin, M. Bayer. Phys. Rev. X, **7**, 021009 (2017).

[116] I.V. Savochkin, M. Jäckl, V.I. Belotelov, I.A. Akimov, M.A. Kozhaev, D.A. Sylgacheva, A.I. Chernov, A.N. Shaposhnikov, A.R. Prokopov, V.N. Berzhansky, D.R. Yakovlev, A.K. Zvezdin, M. Bayer. Sci. Rep., **7** (1), 5668 (2017).

[117] Yu. Hashimoto, S. Daimon, R. Iguchi, Y. Oikawa, K. Shen, K. Sato, D. Bossini, Y. Tabuchi, T. Satoh, B. Hillebrands, G.E.W. Bauer, T. H. Johansen, A. Kirilyuk, T. Rasing, E. Saitoh. Nat. Commun., **8**, Art. num. 15859, (2017).

[118] Y. Hashimoto, D. Bossini, T.H. Johansen, E. Saitoh, A. Kirilyuk, Th. Rasing. Phys. Rev. B, **97**, 140404 (2018).

[119] I. Yoshimine, T. Satoh, R. Iida, A. Stupakiewicz, A. Maziewski, T. Shimura. J. Appl. Phys., **116** (4), 043907 (2014).

[120] I. Yoshimine, Y.Y. Tanaka, T. Shimura, T. Satoh. EPL, **117** (6), 67001 (2017).

[121] N. Ogawa, W. Koshibae, A.J. Beekman, N. Nagaosa, M. Kubota, M. Kawasaki, Y. Tokura. Proc. Natl. Acad. Sci. U.S.A., **112** (29), 8977 (2015).

[122] K. Matsumoto, I. Yoshimine, K. Himeno, T. Shimura, T. Satoh. Phys. Rev. B, **101** (18), 184407 (2020).

[123] T. Hioki, Y. Hashimoto, E. Saitoh. Commun. Phys., **3** (1), 188 (2020).

[124] T. Hioki, R. Tsuboi, T.H. Johansen, Y. Hashimoto, E. Saitoh. Appl. Phys. Lett., **116** (11), 112402 (2020).

[125] N.E. Khokhlov, P.I. Gerevenkov, L.A. Shelukhin, A.V. Azovtsev, N.A. Pertsev, M. Wang, A.W. Rushforth, A.V. Scherbakov, A.M. Kalashnikova. Phys. Rev. Appl., **12**, 044044 (2019).

[126] V.E. Demidov, S.O. Demokritov, D. Birt, B. O'Gorman, M. Tsoi, X. Li. Phys. Rev. B, **80**, 014429 (2009).

[127] Y. Au, T. Davison, E. Ahmad, P.S. Keatley, R.J. Hicken, V.V. Kruglyak. Appl. Phys. Lett., **98** (12), 122506 (2011).

[128] Y. Au, M. Dvornik, T. Davison, E. Ahmad, P.S. Keatley, A. Vansteenkiste, B. van Waeyenberge, V.V. Kruglyak. Phys. Rev. Lett., **110**, 097201 (2013).

[129] Ia.A. Filatov, P.I. Gerevenkov, M. Wang, A.W. Rushforth, A.M. Kalashnikova, N.E. Khokhlov. J. Phys., Conf. Ser., **1697**, 012193 (2020).

[130] N.E. Khokhlov, A.E. Khramova, Ia.A. Filatov, P.I. Gerevenkov, B.A. Klinskaya, A.M. Kalashnikova. J. Magn. Magn. Mater., **534**, 168018 (2021).

[131] O. Kolokoltsev, N. Qureshi, E. Mejía-Uriarte, C.L. Ordóñez Romero. J. Appl. Phys., **112** (1), 013902 (2012).

[132] O. Kolokoltsev, I. Gómez-Arista, N. Qureshi, A. Acevedo, C.L. Ordóñez Romero, A. Grishin. J. Magn. Magn. Mater., **377**, 1 (2015).

[133] S. Gupta, R. Medwal, D. Kodama, K. Kondou, Y. Otani, Y. Fukuma. Appl. Phys. Lett., **110** (2), 022404 (2017).

[134] M. Jaris, W. Yang, C. Berk, H. Schmidt. Phys. Rev. B, **101**, 214421 (2020).

[135] G. Varvaro, F. Casoli, and Eds. *Ultra-high-density Magnetic Recording, Storage Materials and Media Designs* (CRC press, Boca Raton, FL, 2016)

[136] C.L. Degen, M. Poggio, H.J. Mamin, C.T. Rettner, D. Rugar. Proc. Natl. Acad. Sci. U.S.A., **106** (5), 1313 (2009).

[137] D.D. Awschalom, C.H.R. Du, R. He, J. Heremans, A. Hoffmann, J. Hou, H. Kurebayashi, Y. Li, L. Liu, V. Novosad, J. Sklenar, S. Sullivan, D. Sun, H. Tang, V. Tyberkevych, C. Trevillian, A.W. Tsen, L. Weiss, W. Zhang, X. Zhang, L. Zhao, Ch.W. Zollitsch. *Quantum Engineering with Hybrid Magnonics Systems and Materials*. IEEE Transactions on Quant. Engineer., 1−1 (2021).

[138] L. Hou, M. Haji, J.H. Marsh, A.C. Bryce. Opt. Express, **19** (26), B75 (2011).

[139] M. Kobecki, G. Tandoi, E. Di Gaetano, M. Sorel, A.V. Scherbakov, T. Czerniuk, C. Schneider, M. Kamp, S. Höfling, A.V. Akimov, M. Bayer. Ultrasonics, **106**, 106150 (2020).

[140] M. Kobecki, A.V. Scherbakov, T.L. Linnik, S.M. Kukhtaruk, V.E. Gusev, D.P. Pattnaik, I.A. Akimov, A.W. Rushforth, A.V. Akimov, M. Bayer. Nat. Commun., **11** (1), 4130 (2020).

[141] C. Boeglin, E. Beaurepaire, V. Halté, V. López-Flores, C. Stamm, N. Pontius, H.A. Dürr, J-Y. Bigot. Nature, **465** (7297), 468 (2010).

[142] S. Baierl, M. Hohenleutner, T. Kampfrath, A.K.A.K. Zvezdin, A.V. Kimel, R. Huber, R.V. Mikhaylovskiy. Nat. Photonics, **10** (11), 715 (2016).

[143] S. Schlauderer, C. Lange, S. Baierl, T. Ebnet, C.P. Schmid, D.C. Valovcin, A.K. Zvezdin, A.V. Kimel, R.V. Mikhaylovskiy, R. Huber. Nature, **569** (7756), 383 (2019).

[144] D. Afanasiev, J.R. Hortensius, B.A. Ivanov, A. Sasani, E. Bousquet, Y.M. Blanter, R.V. Mikhaylovskiy, A.V. Kimel, A.D. Caviglia. Nat. Mater., **20** (5), 607 (2021).

[145] M. Forst, C. Manzoni, S. Kaiser, Y. Tomioka, Y. Tokura, R. Merlin, A. Cavalleri. Nat. Phys., **7** (11), 854 (2011).

[146] A. Stupakiewicz, C.S. Davies, K. Szerenos, D. Afanasiev, K.S. Rabinovich, A.V. Boris, A. Caviglia, A.V. Kimel, A. Kirilyuk. Nat. Phys., **17** (4), 489 (2021).